Dissertation

Inflammatory responses in myocardial infarction remodeling

submitted by

Dr. med. univ.

Cara Lavinia Shirin Rech, MA MSc

for the academic degree

Doctor of Philosophy (PhD)

at the

Medical University of Graz

performed at

Division of Cardiology,

Department of Internal Medicine

under the Supervision of

Assoc.-Prof. Priv.-Doz. Dr. med. univ. et scient. med. Peter Rainer

2023

Statutory Declaration and Disclosures

Parts of this thesis have been published in

Rech, L[1]; Rainer, PP[1,2]. The innate immune cGAS-STING-Pathway in Cardiovascular Diseases – A mini Review. *Front. Cardiovasc. Med. 2021 July 26; 715903*

1 Division of Cardiology, Department of Internal Medicine, Medical University of Graz, Graz, Austria
2 BioTechMed Graz, Graz Austria

Rech, L[1]; Abdellatif, M[1]; Pöttler, M[1]; Stangl, V[2]; Mabotuwana, N[3,4]; Hardy, S[3,4] and Rainer, PP[1,5]. Small molecule STING inhibition improves myocardial infarction remodeling. *Life Sciences 2022 (291) 120263*

1 Department of Internal medicine, Division of Cardiology, Medical University of Graz, Graz, Austria
2 Diagnostic and Research Institute of Pathology, Medical University of Graz, Graz, Austria
3 School of Medicine and Public Health, The University of Newcastle, Callaghan, Australia
4 Hunter Medical Research Institute, New Lambton Heights, Australia
5 BioTechMed Graz, Graz, Austria

Mahmoud Abdellatif, Maria Pöttler, Verena Stangl, Nishani Mabotuwana, Sean Hardy, and Peter P. Rainer actively contributed to the results of this thesis and the publication resulting from the thesis project. All co-authors have explicitly agreed to the use of their data in this thesis.

I hereby declare that this dissertation is my own original work and that I have fully acknowledged by name all of those individuals and organisations that have contributed to the research for this dissertation. Due acknowledgement has been made in the text to all other material used. Throughout this dissertation and in all related publications, I followed the guidelines of "Good Scientific Practice".

Cambridge, 26.02.2023 *Dr. Lavinia Rech, eh*

Acknowledgement

First of all, I would like to thank my supervisor DDr. Peter Rainer. Not only did he accompany me through the ups and downs of this study, but he also awakened my love for research, which I now no longer want to miss in my life. Furthermore, I would like to thank Dr. Ruth Birner-Grünberger and Dr. Dirk von Lewinski, who gave me essential input to this thesis as part of my thesis committee.

A huge thank you goes to my lab team. You made my time unforgettable. You shared my failures and, more importantly, my successes. You showed me what it means to be a team.

A special thanks also go to my close friends Markus, Theresa, Melanie and Beatrice, who have been with me on this journey and the following one, listening to my problems and working with me on solutions. Love you.

My most important thanks go to my parents, who have accompanied and supported me through what is now my fourth degree and continue to support me unconditionally, for which I am incredibly grateful. I love you

To another one ;-)

This thesis was funded by the ERA-CVD and the Austrian Science Fund (FWF) [AIR-MI project: I 4168-B to Peter P. Rainer] and the Medical University of Graz through the PhD Program "Molecular Medicine". The study abroad in the lab of Ingeborg Friehs at the Boston Children's Hospital, Massachusetts, United States, was supported by the Austrian Marshall Plan Foundation.

Zusammenfassung / Abstract in German

Herz-Kreislauf-Erkrankungen sind eine der größten Belastungen unserer Zeit. Einen großen Teil davon bilden die ischämischen Erkrankungen, einschließlich des Myokardinfarkts (MI). Der Verschluss von Herzkranzgefäßen führt zu einer Hypoxie im Herzmuskel und verursacht dadurch das Absterben von Kardiomyozyten. Entzündliche Prozesse sind erforderlich zur Wundheilung und der Beseitigung von Zelltrümmern. Diese Prozesse stehen in einem fein-regulierten Gleichgewicht zwischen einer entzündungsfördernden und einer reparationsfördernden Phase. Eine zu ausgedehnte Entzündungsphase fördert jedoch die Ausdehnung des Infarkts und einen ungünstigen Umbauprozess mit folgender Herzinsuffizienz. An der Initiierung einer Entzündungsreaktion ist der cGAS-STING-Signalweg beteiligt. Er ist Teil der Immunabwehr des angeborenen Immunsystems. Das Enzym cGAS erkennt DNS, welche sich nicht im Zellkern bzw. in den Mitochondrien befindet, und aktiviert das nachgeschaltete STING Enzym, welches wiederum zur Transkription von Typ I Interferon (IFN) führt. Jüngste Arbeiten haben gezeigt, dass dieser Signalweg auch nach einem Herzinfarkt aktiv ist und dass seine genetische Beeinflussung durch Inaktivierung zu einer verbesserten Ventrikelfunktion führt. Daher untersuchten wir, ob eine pharmakologische Hemmung dieses Signalwegs nach einem Herzinfarkt ebenfalls schützend wirkt.

Dazu haben wir männliche C57/BL6J-Mäuse operiert, um einen Herzinfarkt zu induzieren, oder Scheinoperation als Kontrollen durchgeführt. Anschließend injizierten wir diesen Mäusen täglich i.p. einen STING-Inhibitor oder eine Kontrollsubstanz. Mithilfe von Echokardiographie, Histologie und qPCR wurden die Veränderungen des Myokardumbaus in Abhängigkeit vom Inhibitor bewertet.

In einem permanenten Ligaturmodell führte die STING-Inhibition nicht zu einer Verringerung der Sterblichkeit aufgrund von Myokardrupturen. Auch bei den IFN-induzierten Genen (*Ifi44, Ifit2, Cxcl10, Isg15*) wurden nach 4 Tagen keine signifikanten Unterschiede festgestellt. Im Ischämie/Reperfusionsmodell (I/R) war die Infarktgröße an Tag 1 vergleichbar. Nach drei Wochen täglicher Behandlung verringerten sich Infarktausdehnung und Narbenbildung, die systolische Funktion des linken Ventrikels stieg auf Werte, die sich den Normalwerten annäherten, und die Myokardhypertrophie nahm ab.

Darüber hinaus konnten bei den IFN-induzierten Genen *Ifi44* und *Cxcl10* eine signifikante Abnahme der Expression in der Infarktzone beobachtet werden und zusätzlich ein abnehmender Trend bei *Ifit2* und *Isg15*.

Zusammenfassend lässt sich sagen, dass die selektive Hemmung von STING nach einem Myokardinfarkt das Potenzial hat, die Wundheilungsreaktionen und den pathologischen Umbau zu verbessern und dadurch die negativen Entwicklung einer ischämischen Herzinsuffizienz abzuschwächen.

Abstract

Cardiovascular diseases (CVDs) are one of the tremendous burdens of today. Within these, a major group encompass ischemic heart diseases, including myocardial infarction (MI). Occlusion of coronary vessels leads to hypoxia in the myocardium and causes the death of cardiomyocytes. Clean-up of cell debris and wound healing needs inflammatory processes. These processes are precisely balanced between a pro-inflammatory and a pro-reparatory phase. Extensive inflammation, however, promotes infarct expansion and adverse remodeling. Involved in recognising the need for an inflammatory response is the cGAS-STING pathway. It is part of the first-line immune defence of the innate immune system. The enzyme cGAS senses DNA, which is not located in the nucleus or the mitochondria, and activates downstream STING, leading to the transcription of type I interferon (IFN). Recent papers demonstrated that this pathway is also active following MI and that its genetic targeting though inactivation leads to improved ventricular function. Thus, we investigated if pharmacologic pathway inhibition is protective after MI.

Therefore, we operated C57/BL6J male mice to induce MI and used sham-operated mice as controls. Further, we injected these mice daily i.p. with a STING-inhibitor or vehicle control. We used echocardiography, histology, and qPCR to assess changes in myocardial remodeling based on STING inhibition.

In a permanent ligation model, STING inhibition did not reduce mortality due to myocardial rupture. Further, the IFN-induced genes (*Ifi44, Ifit2, Cxcl10, Isg15*) did not show significant differences after four days. In ischemic/reperfusion (I/R) model infarct size was comparable at day 1. After three weeks of daily treatment, we observed decreased infarct expansion and scarring, increased left ventricular systolic function to levels approaching normal values, and reduced myocardial hypertrophy. Additionally, a significant decrease in molecular levels in the infarct zone could be observed in the IFN-induced genes *Ifi44* and *Cxcl10* and further a decreasing trend in *Ifit2* and *Isg15.*

In conclusion, selective small-molecule STING inhibition after myocardial infarction has the potential to improve wound healing responses and pathological remodeling and thereby attenuate the negative development of ischemic heart failure.

Table of Contents

Abbreviations and Definitions

Italic abbreviations represent genes; abbreviations with capital letters only are for human materials, and the first capital, otherwise small, represents mouse and rat.

18s rRNA	18s ribosomal RNA (Small ribosomal subunit component)
AMP	adeninmonophosphate
ANOVA	analysis of variance
ARR	area at risk
αSMA	alpha-smooth muscle actin
AAV9	adeno-associated virus 9
BW	body weight
Ccl17	CC motif chemokine ligand 17
CD163	cluster of differentiation 163
cDNA	complementary deoxyribonucleic acid
cGAS /*cGAS*	cyclic GMP-AMP synthase
cGAMP	cyclic guanine-adenine-monophosphate
CK-MB	Creatininkinase – muscle-brain-type
Col1a1	collagen type 1 alpha 1
Col1a2	collagen type 1 alpha 2
Col3a1	collagen type 3 alpha 1
COVID-19	coronavirus disease of 2019
CSA	cross-sectional area
CVD	cardiovascular disease
Cxcl10 / *CXCL10* / CXCL10	chemokine (C-X-C-motif) ligand 10
DAMP	damage-associated molecular patterns
dH_2O	distilled water
DNA	deoxyribonucleic acid
ECG	electrocardiogram
EDA	endocardial area diastole
EndMT	endothelial-to-mesenchymal transition
EF	ejection fraction
ER	endoplasmic reticulum
ESA	endocardial area systole

FAC	endocardial fractional area change
FFPE	formalin-fixed paraffin-embedded
FS	fractional shortening
GMP	guanine monophosphate
HF	heart failure
Hmbs	hydroxymethylbilane synthase
Ifi44	interferon-induced protein 44
Ifit2	interferon-induced protein with tetratricopeptide repeats 2
Ifit3	interferon-induced protein with tetratricopeptide repeats 3
IFN / *Ifn*	interferon
Ifnα / Ifnα	interferon alpha
Ifnβ / Ifnβ	interferon beta
IFN- γ	interferon gamma
IL	Interleukin
IL-1	interleukin 1
Il1α	interleukin 1 alpha
Il1β / *IL-1β* / IL-1β	interleukin 1 beta
Il6 / *IL-6* / IL-6	interleukin 6
Il-8	interleukin 8
IL-10	interleukin 10
IL-18	interleukin 18
i.p.	intraperitoneal
I/R	ischemia/reperfusion
IRF	interferon releasing factor
IRF3 / *IRF3* / *Irf3*	interferon releasing factor 3
Isg15	ubiquitin-like modifier interferon-stimulated gene 15
KO	knock-out
LAD	left anterior descending artery
LPS	lipopolysaccharide
LV	left ventricle
LVAD	left ventricular assist device
LVIDd	left ventricular inner diameter in diastole
LVIDs	left ventricular inner diameter in systole

µg	microgram
µl	microliter
MACE	major adverse cardiac events
mg	milligram
MI	myocardial infarction
ml	millilitre
Myh6	myosin, heavy polypeptide 6, cardiac muscle, alpha
Myh7	myosin, heavy polypeptide 7, cardiac muscle, beta
NF-κB	nuclear factor kappa-light-chain-enhancer of activated B-cells
Nppa	natriuretic peptide type A
Nppb	natriuretic peptide type B
ns	non-significant ($p > 0.05$)
PBS	phosphate-buffered saline
PCI	percutaneous coronary intervention
PWd	posterior wall diastole
PWs	posterior wall systole
SARS-CoV2	severe acute respiratory syndrome coronavirus 2
s.c.	subcutaneous
SIC	sepsis-induced cardiomyopathy
siRNA	small-interfering ribonucleic acid
SNAIL	zinc finger protein snail family transcriptional repressor 1
STING / *STING*	stimulator of interferon genes
TAC	transverse aortic constriction
TBK1	TANK-binding kinase 1
TGF	transforming growth factor
TGFβ / Tgfβ	transforming growth factor beta
Tgfβ1	transforming growth factor beta 1
Tgfβ2	transforming growth factor beta 2
TNF, Tnf	tumor necrosis factor
Tnfα / TNFα / Tnfα	tumor necrosis factor alpha
TTC	2,3,5-Triphenyl tetrazolium chloride
WGA	wheat germ agglutinin
WT	wild-type

List of Figures

List of Tables

1 Introduction

Cardiovascular diseases (CVDs) are one of the tremendous burdens of today. With nearly 18 million people each year (1, 2), they are the most common cause of death worldwide (3). In the 57 member countries of the European Society of Cardiology, the incidence of CVD was 12.7 million people, and the prevalence was over 113 million in 2019 (4). One of the major entities in CVDs is myocardial infarction (MI). In the U.S. in 2018, over 100.000 people died because of an acute MI (5). Different risk factors are increasing the likelihood of a MI. Moreover, even when we are getting better in risk stratification, patients undergoing percutaneous coronary intervention (PCI) show more and more risk factors, like diabetes or hypertension, from year to year (6). After patients survive a MI, the risk of developing chronic heart failure (HF) increases. Despite PCI lowering these levels, 28% of patients still develop HF (7). Therefore, it is necessary to understand the underlying mechanisms better. One main focus is the treatment of MI and a better understanding of the underlying mechanisms of cardiac remodeling after MI. It is worth mentioning that two main phases after the MI are essential for the healing process. First is the pro-inflammatory phase, which cleans the infarcted area of debris and dead cells — followed by the secondary, the pro-reparative phase, for repairing the infarcted area. Both phases are accompanied by specific inflammatory cells and cyto- and chemokines (**Fig 1.**). However, while both phases are necessary, prolonging or expanding inflammatory response is associated with worse remodeling after MI (8).

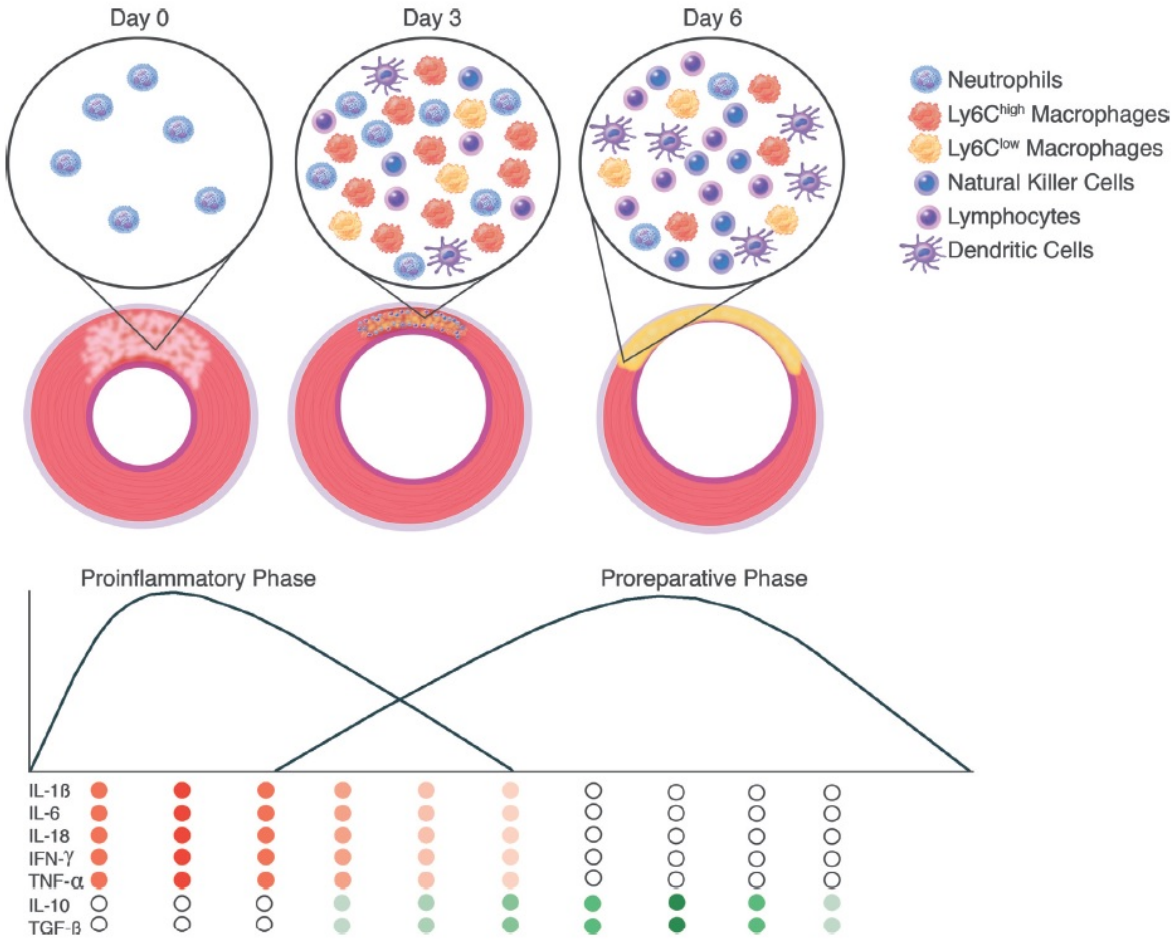

Figure 1: Inflammation and Remodeling after Acute Myocardial Infarction: Simplified Depiction of Cellular and Cytokine Responses
Reproduced from Westman, PC et al. J Am Coll Cardiol. 2016;67(17):2050-60 (9) with permission of Elsevier (license Number 5487760509510

1.1 The inflammatory responses after myocardial infarction

Coronary occlusions lead to a decreased level of oxygen in the myocardium. Further, cardiomyocytes in the hypoxic area die, and necrosis and cell debris are significant findings (10) . Inflammatory processes are responsible for the cleaning and reparation of these wounds (11) . It became more and more evident that the balance of the pro-inflammatory phase of cleaning and the pro-reparatory phase of cardiac repair is mandatory for a good outcome after myocardial infarction.

The healing process starts with the pro-inflammatory phase. Different inflammatory cell types are involved in different stages, starting with mast cells and neutrophils, originating from the innate immune system and migrating into the affected myocardium (9, 12, 13) . Cells of the adaptive immune system follow a couple of days later (14) . These immune cells are recruited to the infarcted area by different signals. These signals are released from

necrotic cells or damaged extracellular matrix, known as damage-associated molecular patterns (DAMP) (8, 10, 15) . Additionally, cardiomyocytes and resident macrophages release cyto- and chemokines like Il-1, Il-6 and Tnfα (9, 12) . $CD4^+$-T cells from the adaptive immune system follow. However, these cells seem to behave differently due to the type of MI. Based on *in-vivo* experiments, on the one hand, they are increasing the infarct size in a permanent ligation model (16, 17) . On the other hand, Hoffman et al. showed that in a reperfusion model, different types of $CD4^+$-T cells are required for scar formation to prevent left heart dilatation and rupture (14, 16) . Moreover, even B-cells are involved in the post-ischemic process, with a distinct subset in the healing myocardium (18) . The impact of B-cells after MI is supported by the finding that using the anti-CD20 antibody Rituximab as cancer treatment reduces inflammation and infarct size after MI and improves cardiac function (19, 20) .

Though the pro-inflammatory phase is necessary, if prolonged, it will lead to increased risks for cardiac ruptures and aneurysms (8, 11) . Therefore, the shift to the pro-reparatory phase is essential. In this phase leading cyto- and chemokines are Il-10 and Tgfβ (9, 21, 22) . The main driver of myocardial repair is the cardiac fibroblast, which differentiates into myofibroblast and results in scar formation (11, 23, 24) . Nonetheless, a prolonged pro-reparatory phase increases collagen storage in the myocardium and decreases systolic function (23) .

Likewise, the immune cells must be in the right balance with each other. For instance, type 1-like macrophages are mainly pro-inflammatory and required, in the beginning, to clean up damaged tissue, while type 2-like macrophages, usually the anti-inflammatory type, are essential for the reparation of the tissue (25–27) . Early trials with non-specific anti-inflammatory therapies after MI showed divergent successes. However, low-dose Colchicine after MI and in stabile angina reduced the risk of following cardiocerebrovascular events (28, 29) .

This balance also applies to cytokines. Mice studies show that overexpression of Tnfα results in a decreased ejection fraction (EF) (30) , while inhibition of Tnfα in a preclinical model of myocardial infarction leads to preserved cardiac functions (31) . However, inhibition of TNFα increased platelet activation in a clinical study and was therefore not beneficial in patients (27, 32) . Further, the interleukins *Il-1α* and *Il-1β* are upregulated in dying cardiomyocytes and after experimental acute myocardial infarction (24, 27) .

Additionally, different cardiomyopathies lead to an increase of the pro-inflammatory cytokines like Il-1, Il-6, Il-8 and Tnf via DAMPs and can increase heart failure risk (27, 33, 34). That selective anti-inflammatory treatment can be beneficial showed the CANTOS trial. There were patients treated with the anti-IL-1β antibody Canakinumab for secondary prophylaxis after MI. It significantly reduced C-reactive protein and IL-6 and further in moderate and high doses, leading to a 15% reduction of primary MACE endpoints (35).

Another approach would be upstream of the cytokines-release pathway. For instance, in the heart, the transcription factor NF-κB (27, 36, 37), i.e., associated with allograft rejection and ischemic injuries in heart transplantations (27, 38). Other transcription factors involved in CVDs are interferon (IFN) regulatory factors (IRF). As their name already implies, they are involved in the expression of IFNs (27, 39). One curious type of these transcription factors is IRF-3. It is the key transcription factor of the cGAS-STING-pathway (27, 40).

1.2 The cGAS-STING-pathway

Our immune system exists of the innate system and the adaptive immune system. The former represents our first-line defence. Natural killer cells, dendritic cells and phagocytes, such as neutrophils, eosinophils, and macrophages, are the cellular components of the innate immune system (27, 41, 42). Cytokines, like IFNs, interleukins (ILs), tumour necrosis factors (TNFs) and transforming growth factors (TGFs), natural antibodies and the complement system form the humoral system of the innate immune system (27, 42–44). Different molecules can trigger this system. These are paraphrased as pathogen-associated molecular patterns (PAMPs) and damage-associated molecular patterns (DAMPs). For instance, a PAMP would be lipopolysaccharide (LPS), an endotoxin of the membrane of gram-negative bacteria, which leads to a strong inflammatory response (45). Cytosolic DNA, released from mitochondria or nucleus by stress or tissue damage, displays a potential DAMP (27, 44, 46) and leads to a release of IFN (22, 27, 47).

One pathway for sensing PAMPs and DAMPs and activating an inflammatory response is the cGAS-STING-pathway (**Fig. 2**). The cytosolic GMP-AMP synthase (cGAS) is a 63kDa protein localised in the cytoplasm during the cell cycle's interphase (27, 48).

After sensing, cGAS releases the second messenger cyclic-GMP-AMP (cGAMP) by transforming ATP and GTP after sensing double-strand DNA (27, 49–60) . This second messenger activates the stimulating of interferon genes (STING) receptor (27, 40, 49, 52, 58, 60, 61) . STING is a receptor protein localised at the endoplasmic reticulum (ER), with three isoforms ranging from 9 – 34 kDa (27, 62) . The binding of cGAMP leads to the multimerization of the STING receptors and performs a configuration change (63) . This change enables the activation of TANK-binding kinase 1 (TBK1). Further, activated TBK1 phosphorylates the interferon releasing factor 3 (IRF3) (27, 40, 49, 59, 60, 64–66) . This transcription factor IRF3 then finally translocates into the nucleus and activates there the transcription of type I IFNs (27, 40, 49) .

Even ER stress activates STING and IRF3, which leads to autophagy in these cells (27, 55, 67) . Nonetheless, if survival is not reasonable, STING activates T-cells. After that, these T-cells induce a type I IFN response, cell stress, and apoptosis (27, 68) . Surprisingly, this mechanism is still active in T-cell-derived cancer cells. Therefore, it displays exciting possibilities for future therapies (27, 69) . Using an agonist of the cGAS-STING pathway increases apoptosis in malignant B cells and improves the outcome of solid tumours (27, 70–72) . Additionally, it is a feasible treatment against infections, for instance, Hepatitis B (73) .

However, increased inflammatory processes cause problems as well. This also applies to the cGAS-STING pathway. For example, the STING-associated vasculopathy with onset in infancy (SAVI) shows a couple of severe symptoms like vasculopathy and ulcers due to uncontrolled inflammation (74) . Consequently, regulatory mechanisms are unavoidable. One mechanism is cytosolic deoxyribonuclease at a low level. It destroys minor amounts of DNA in the cytosol and prevents the entire inflammatory cascade is fomenting (27, 75) . Another protective mechanism is the cell's compartmentation to avoid nuclear DNA sensing by cytosolic sensors, as the regulatory capacity is limited (27, 75) . A substantial amount of DNA can be released into the cytosol by genomic instability and nucleic damages, where cGAS can sense it (27, 60, 61, 76) . Besides nuclear DNA, this also applies to mitochondrial DNA (27, 77) . The increased amount of self-DNA, which activates the cGAS-STING pathway, is further associated with autoimmune diseases, for instance, Ataxia Telangiectasia, systemic Lupus erythematosus or Aicardi-Goutières syndrome (27, 55, 58, 76, 78, 79) .

Given that the patient's regulatory mechanisms are sometimes inadequate, a therapeutic approach is necessary. Different pharmacological approaches are already available in research (**Fig. 2**) (80) . One is the inhibition of cGAS. Binding to the catalytic site of cGAS, inhibitors like PF-06928125 or RU521 prevent the formation of cGAMP (81–83) . Another possibility is the inhibition of STING. The STING multimer assembly is necessary for the phosphorylation of TBK1. By inhibiting cysteine palmitoylation, STING inhibitors such as nitrofuran derivatives and indole ureas, which bind covalently to STING, prevent this multimer assembly (63, 81, 84) . Specific binding to mouse STING (mmSTING) with a good inhibition of the pathway can be received by the nitrofuran C-176 or C-178 (84) . The indole urea inhibitor H-151 antagonises mmSTING and human STING (hsSTING) palmitoylation and reaches therapeutic drug concentrations in mice (63, 84) .

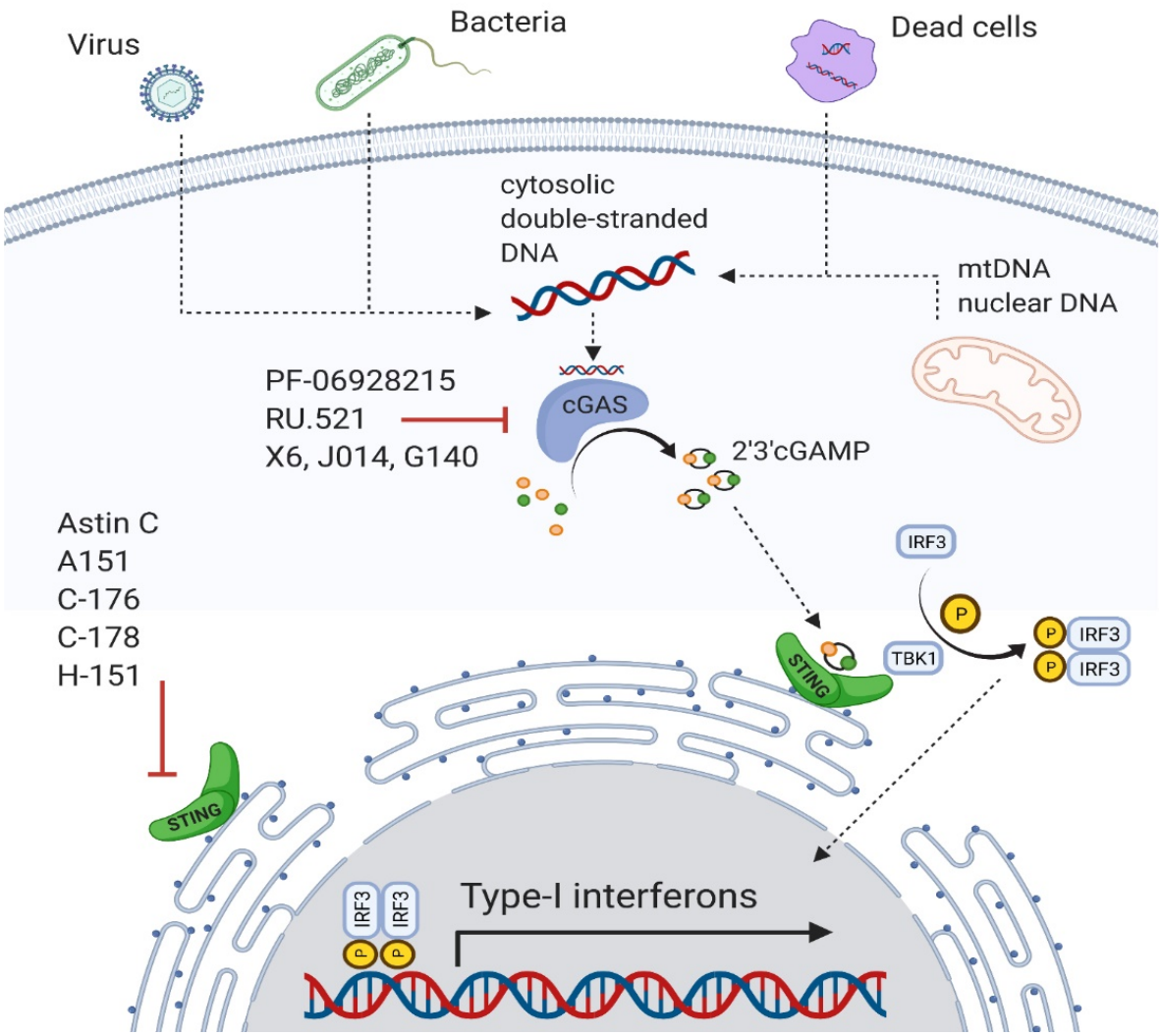

Figure 2: Scheme of the cGAS-STING-Pathway and inhibitors
Reproduced from Rech ,L et Rainer, PP Front Cardiovasc Med,2021:715903 with permission under CC BY 4.0 (27)

1.3 cGAS-STING in the heart

1.3.1 Infections

In an *in-vitro* model of sepsis-induced cardiomyopathy (SIC) in neonatal rat cardiomyocytes, Li et al. illustrated an increase of STING and phosphorylated Irf3. (85) . Additionally, they induced SIC with LPS in an *in-vivo* model of STING knock-out (KO) mice. These mice showed improved ejection fraction (EF), fractional shortening (FS), and survival, together with reduced levels of CK-MB, Il-1β, and Tnfα in these KO mice (27, 85) . In LPS-induced SIC in WT mice, a similar effect was seen using the small cGAS inhibitor RU.521 (27, 86) .

Trypanosoma cruzi is the virus responsible for Chagas cardiomyopathy. Cells infected with this virus drive macrophages to raise levels of *Il-1β*, *Il-6* and *Tnfα*. Different inhibitors, like the cGAS inhibitor PF-06928215 (27, 87) , could alleviate this.

Further, there is speculation that COVID-19 infection may lead to prolonged cGAS-STING pathway activation in leucocytes (88) , and increased leukocyte infiltration was present in most COVID-19 patients' hearts in an autopsy study (27, 89) . In a lung-on-chip model, Domizio et al. demonstrated that infection with SARS-CoV2 activates the cGAS-STING pathway in endothelial cells (90) . This is accomplished by the spike protein-induced cell fusion, which leads to nuclei damage and its activation of the cGAS-STING pathway (91) .

1.3.2 Heart Failure

Heart failure (HF) describes a clinical syndrome of many CVDs, such as hypertension or ischemia, in their end-stage progression (27, 92) . An *in-vivo* model of HF is the induction of a non-ischemic pressure overload through transverse aortic constriction (TAC) (93) . An *in-vitro* model of HF is the stimulation with angiotensin II to induce hypertrophy in cardiomyocytes (94) . Zhang et al. investigated that the *in-vivo* model displays fibrosis, cardiac hypertrophy, and dysfunction, together with increased levels of STING, Ifnα, and Ifnβ. These findings could also be observed in human samples of dilative and hypertrophic cardiomyopathies. In STING-KO mice, levels returned to baseline levels (27, 95) .

In the *in-vitro* model with neonatal rat cardiomyocytes, stimulation with angiotensin II presented rising levels of *STING*, *Ifnα*, and *Ifnβ*. Inhibition with a siRNA against STING appeared with decreased levels of *Il-6*, *Il-1β*, *Tnfα*, *Ifnα*, and *Ifnβ* (27, 95) .
Furthermore, the increased expression of *cGAS*, *STING*, *Ifn*, and IFN-induced chemokines *Cxcl10*, *Ifit3*, and *Isg15* was observed by Hu et al. three days after TAC, too. Silencing cGAS with an adeno-associated virus 9 (AAV9) significantly reduces cardiac remodelling and fibrosis (27, 96, 97) .

1.3.3 Myocardial Infarction

Besides cardiac infection and non-ischemic heart failure, the cGAS-STING pathway is also involved in response to myocardial infarction. Increased expression levels of *cGAS*, *STING*, *IRF3* and *CXCL10* were observed (84, 98–100) . This was attenuated by using knockout models for pathway members such as cGAS, STING, or IRF3. Interestingly, cGAS knockout ($cGAS^{-/-}$) did not reduce the universal pro-inflammatory cytokines *Il-1β*, *Tnfα*, and *Il-6* (27, 98) . However, $cGAS^{-/-}$ and IRF3 KO mice ($IRF3^{-/-}$) presented improved survival and systolic function after non-reperfused MI (98, 99) . STING-deficient mice ($STING^{gt/gt}$) did not demonstrate increased survival or systolic function (99) . Contrastingly, using the small molecule STING inhibitor H-151 ameliorated the systolic function in non-perfused and reperfused MI (84, 100) .
With a parabiosis experiment and scRNAseq data, King et al. demonstrated that monocyte-derived cardiac macrophages that phagocytose cell debris after MI are the relevant cells of the increased expressions of IRF3-dependent genes (27, 99) . This was confirmed by Hu et al., who showed an increase of macrophages in the heart after MI and a decreased number after using a STING inhibitor (100) . Additionally, Cao et al. treated wild-type (WT) and $cGAS^{-/-}$ human macrophages with DNA to stimulate *in-vitro* IFN expression. While $cGAS^{-/-}$ macrophages produced no *CXCL10*, it was expressed in WT macrophages (27, 98) . Moreover, *Cxcl10* is associated with M1-like polarisation, the pro-inflammatory type of macrophage (27, 98, 101) . In contrast, M2 markers (pro-reparative) like *CD163*, *Il-10*, and *Ccl17* were increased in $cGAS^{-/-}$ animals (27, 98, 101) . Furthermore, Cao et al. also investigated that increased levels of cGAS and CXCL10 occur in human end-stage ischemic HF patients (27, 98) . Along with this, mechanical circulatory support via left ventricular assist devices (LVADs) in these patients attenuated these levels near to normal (27, 98) .

1.4 Summary

Necrosis in myocardial tissue triggers inflammation and wound healing. This is necessary to clear the wound of debris and dead cells and activate pathways for tissue reparation. Nevertheless, a prolongation or expansion of the inflammatory response is associated with worse remodeling after MI (8). Many different cytokines and chemokines manage inflammation in different phases. In a pro-inflammatory phase, cytokines like IL-1β, IL-6, IL-18, IFN- γ, and TNFα are active, while in the pro-reparative phase, levels of, e.g. IL-10 and TGF-β increase (9).

Essential in inflammation caused by cell death are damage-associated molecular patterns (DAMPs) (15). In the case of damaged cells, double-stranded DNA (dsDNA), usually localised separately in the nucleus, can be found in the cytosolic space and act as a DAMP. This cytosolic dsDNA is sensed by the cyclic GMP-AMP synthase, known as cGAS (49, 54, 58). In turn, cGAS releases the second messenger cyclic adenosine monophosphate-guanosine monophosphate (cGAMP), which activates the endoplasmic-reticulum-resident protein stimulator of interferon genes (STING) (58, 102). The effect of this is the phosphorylation of the Interferon regulatory factor 3 (IRF3), which is a transcription factor for type I interferon. It is already observed that this pathway is activated after MI and that cGAS and IRF3 knockout mice had improved survival after MI (98, 99). Using inhibitors interrupting this pathway is the logical consequence of testing potential translation. A small molecule inhibiting cGAS successfully reduced brain injuries after stroke (103). Further, STING siRNA, inhibiting the expression of the STING receptor, improved the outcome and survival in sepsis-induced cardiomyopathy (85).

The STING inhibitors C-178 and H-151 are binding covalently to STING. Further, H-151 is potent for the mouse and human STING (63). Thus, targeting this inflammatory pathway holds excellent potential in post-MI remodelling for translational research.

1.5 Hypothesis and aim

We hypothesized that small molecule STING inhibition decreases expression levels of IFN-induced chemokines *Ifi44*, *Ifit2*, *Cxcl10* and *Isg15* in the setting of MI. Thereby inhibition of this pathway in the infarcted heart will dampen excessive inflammatory responses and improve cardiac remodeling.

Aims:

1. Development of a murine model for myocardial infarction to test STING inhibition
2. Test effect of STING inhibition on early mortality survival after MI
3. Determine post-ischemic cardiac function and remodeling using STING inhibition
4. Asses the inflammatory responses of STING inhibition after MI

2 Material and Methods

2.1 Ethics statement

Mouse handling and experiments were performed in agreement with the national and European ethical regulations (Directive 2010/63/E.U.), according to the guidelines of the Federation for Laboratory Animal Science Associations FELASA (104, 105) and approved by the responsible government agencies in Austria (Bundesministerium für Wissenschaft, Forschung und Wirtschaft, BMWFW, Austria: BMWF-66.010/0178-WF/V/3b/2017).

2.2 Animals

On average, 20 weeks-old male C57BL/6J mice purchased from Charles River Laboratories (Sulzfeld, Germany) were used. In total, 91 mice were used for the analysis out of 110, which survived the procedures successfully. Rest died before the end of the experiments or staining procedures failed. Animals were randomly assigned to the experimental groups. Animal experiments are reported following the ARRIVE guidelines (106) .

2.3 Myocardial Infarction Operation

2.3.1 Permanent

A mouse is first placed in an anaesthesia chamber saturated with 5% isoflurane, where it falls asleep within 30-45 seconds. After the initial inhalation of isoflurane anaesthesia has taken effect, etomidate is used to maintain the anaesthesia during endotracheal intubation. Therefore, and for analgesia, a solution of buprenorphine (0.05 mg/kg) and etomidate (10 mg/kg) i.p. is injected (**Tab.1**) (84) .

Then the eyes are creamed with panthenol ointment to keep them moist, and the mouse is fixed to the extremities in a supine position on a warm mat at 37°C with adhesive strips. Orotracheal intubation is performed using a mouse laryngoscope and a non-cuffed plastic tube (20 gauge). Isoflurane flows through this tube in pure oxygen by volume-controlled ventilation (150-250µl, 140-170/min). After correct intubation, the mouse will be turned into a right half-side position. The maintenance concentration of isoflurane is set to 1.5-2.5%. The depth of anaesthesia is checked by the complete extinction of pain reflexes (intertoe reflex) (84) . After local depilation (depilatory cream) and disinfection, a left-thoracic skin incision is made along with the pectoralis major muscle (7-10 mm).

After blunt dissection of the pectoral muscles from the thoracic wall, the fourth intercostal space is opened, then the pericardial sac, and finally, the left anterior descending (LAD) coronary artery is displayed. Ligation is then performed with 7-0 monofilament Prolene. The success is assessed visually by purging the front wall of the heart. The wound is then closed in layers (thorax, skin) using a 6-0 monofilament Prolene suture. Isoflurane inhalation is stopped, and extubation takes place if there is sufficient spontaneous breathing. The total duration of the procedure is 15-20 minutes. The mouse is closely monitored postoperatively in a separate cage in a temperature-controlled environment. Once complete awareness and mobility have been achieved, the mouse is returned to its original cage (84) .

Table 1: Sedo-Analgesia permanent ligation model

weight	Sedo-Analgesia			weight	Sedo-Analgesia		
	total volume	Etomidate (10 mg/kg)	Buprenorphine (0.05 mg/kg)		total volume	Etomidate (10 mg/kg)	Buprenorphine (0.05 mg/kg)
[g]	[µl]	[mg]	[µg]	[g]	[µl]	[mg]	[µg]
20	100	0.20	1.00	**31**	155	0.31	1.55
21	105	0.21	1.05	**32**	160	0.32	1.60
22	110	0.22	1.10	**33**	165	0.33	1.65
23	115	0.23	1.15	**34**	170	0.34	1.70
24	120	0.24	1.20	**35**	175	0.35	1.75
25	125	0.25	1.25	**36**	180	0.36	1.80
26	130	0.26	1.30	**37**	185	0.37	1.85
27	135	0.27	1.35	**38**	190	0.38	1.90
28	140	0.28	1.40	**39**	195	0.39	1.95
29	145	0.29	1.45	**40**	200	0.40	2.00
30	150	0.30	1.50				

2.3.2 Ischemia/Reperfusion Operation

A mouse is first placed in an anaesthesia chamber saturated with 5% isoflurane, where it falls asleep within 30-45 seconds. After initial inhalation of isoflurane anaesthesia has taken effect, etomidate (10 mg/kg) i.p. once is used to maintain the anaesthesia during endotracheal intubation (**Tab. 2**) (84) .

Intubation, positioning and access to the LAD are the same as previously described for the permanent ligation model. A time-limited ligation is then performed with 7-0 monofilament Prolene. Success is assessed visually by purging the anterior wall of the heart. In order to make it easier to loosen the ligature later, a piece of plastic tubing is fixed under the knot. The ligature is maintained for 30 minutes and then released.

The return of the original colouration visually assesses the success. Twenty minutes after ligation, 300µl of a solution of 5% Buprenorphine (0.05mg/kg) in 0,9% sodium chloride is injected for analgesia and fluid substitution. Wound closure and ending of the experiment were according to the previously described procedure for the permanent ligation. The total duration of the procedure is 50-60 minutes (84) .

Table 2: Etomidate substitution I/R ligation model

weight			weight		
	total volume	Etomidate (10 mg/kg)		total volume	Etomidate (10 mg/kg)
[g]	[µl]	[mg]	[g]	[µl]	[mg]
20	100	0.20	**31**	155	0.31
21	105	0.21	**32**	160	0.32
22	110	0.22	**33**	165	0.33
23	115	0.23	**34**	170	0.34
24	120	0.24	**35**	175	0.35
25	125	0.25	**36**	180	0.36
26	130	0.26	**37**	185	0.37
27	135	0.27	**38**	190	0.38
28	140	0.28	**39**	195	0.39
29	145	0.29	**40**	200	0.40
30	150	0.30			

2.3.3 Sham procedure

The control group consists of animals that have undergone a sham operation. For this purpose, the procedure is performed the same way as described above in the permanent model, and the LAD is displayed. However, the LAD is not ligated by a suture following this presentation (84) .

2.3.4 Post-operative care

Buprenorphine i.p. is already administered to the animals during surgery to prevent post-operative wound pain (rapid onset of effect). In addition, the animals are treated with buprenorphine (s.c.) in the first three days postoperatively (0.05 mg/kg). The mice are checked daily for signs of pain, wound infection, bleeding or heart failure. The main parameters used for this purpose: Lack of movement, coat raised, changed breathing, refusal to drink, pus discharge, gaping or missing closure of the wound edges, swelling, shortness of breath and oedema. A scoring system for the comprehensible assessment of the degree of stress was developed (paragraph 8.7, page 48) (84) .

2.4 Treatment

C57BL/6J mice have been treated daily with the STING inhibitor or control substance with 200 µl i.p. treatment solution. These solutions were 10% Tween80 in isotonic saline solution with either 10% DMSO alone (control) or 10% Inhibitor (50mM, provided by Prof. Ablasser, Lausanne, Switzerland) solved in DMSO. The first injection was given at the beginning of the operation procedure. Mice were allocated randomly. In the groups with echocardiography, the mice were assigned to the groups based on the baseline echo to create a similar average mean as initial values. The abbreviations for the groups we used were the following: myocardial infarction with inhibitor treatment: MI-Inhib; group with myocardial infarction with vehicle control: MI-CTL; Sham-operated mice with inhibitor treatment: Sham-Inhib; Sham-operated mice with vehicle control: Sham-CTL. (84)

2.5 Echocardiography

The anaesthesia is performed with the inhalation of anaesthetic isoflurane. Isoflurane is ideally suited due to its low cardiovascular side effects and good controllability. The mouse is first placed in an anaesthesia chamber saturated with 3-4% isoflurane, where it falls asleep within 45-60 seconds. Then, if necessary, the mouse is depilated in the front breast area with a commercially available depilatory cream and fixed to a heated plate with ECG electrodes with adhesive strips in a supine position. A gas supply hose with a suitable plastic cone is placed over the nose. Isoflurane flows through this cone in pure oxygen with a 0.5-1.0% maintenance concentration. The concentration is initially set to 2% and then adapted during the ultrasound examination using the simultaneously measured heart rate for all mice (target rate around 500/min) (84) .

For echocardiography with Vevo 770, the breast area of the fixed mouse is covered with a preheated ultrasound gel, a small transducer (RMV 707B) is placed on the breast wall, and the image is recorded in various positions. The examination takes about 5 to 10 minutes. After the examination, the mice are detached from the fixation and cleaned from the ultrasound gel (84) .

2.6 Infarct size measurement

It starts with an injection of 200 IE heparin i.p. and a waiting time of 20 min. Afterwards, the mouse is anaesthetised with isoflurane in an anaesthesia chamber (5% isoflurane). After reaching a deep anaesthetic (45-60 seconds) and extinguishing pain reflexes (intertoe reflex), the mouse gets rapidly neck dislocated to end vitals. The heart will be removed immediately, and the aorta is cannulated in cold PBS on ice. Then the heart is flushed with cold PBS to remove blood from the vessels. After closing the LAD ligation again (same spot as during operation), Evans blue (1% in H_2O) is injected through the aortic cannula slowly, around 350-400 µl, depending on the colouring of the myocardium (84) .

Afterwards, the heart is frozen at -20°C for 5 minutes for a better cutting option. With a Zivic heart slicer, the heart is cut into 1mm sections. Each slice is weighted and then incubated in TTC (1,5% in PBS) at 37°C for 15 min. Then it is removed and fixed in formalin (4%) at room temperature for 90 minutes. Finally, pictures of both sides of the slices were made with an Olympus SZX12 microscope in 8x magnification and a DP21 Olympus camera. Images were analysed with the ImageJ software to quantify the infarct size and the area at risk (84) .

2.7 Quantitative real-time polymerase chain reaction (qPCR) analysis

According to the manual, RNA from the remote and infarct zone (infarct area and area at risk) of fresh frozen heart tissue was isolated using QIAzol lysis reagent and RNeasy kit (protocol paragraph 8.3, page 45). RNA was quantified using a NanoDrop 2000c. According to the manufacturer's instructions, the transcription into cDNA was performed using the QuantiTect Reverse Transcription Kit (protocol paragraph 8.4, page 46).

Reverse transcripts were analysed using Bio-Rad CFX384/CFX96 Detection System with SsoAdvanced Universal SYBR Green Supermix and primers designed by the study team (**Tab. 3**; protocol paragraph 8.5, page 46) and purchased by Ingenetix (Austria). Primer efficiency was calculated using the CFX Manager software from Bio-Rad, after performing a dilution series for each primer (see **Tab. 6**, paragraph 8.6, page 47)

All reactions were performed in triplicates. Analysis of the gene expression levels was efficiently corrected and normalised to the reference genes 18s ribosomal RNA (*18s*) and hydroxymethylbilane synthase (*Hmbs*) and calculated with the ΔΔCt method. Graphs were shown in the bars according to the $2^{-\Delta\Delta Ct}$ method and normalised to their control.

Table 3: Primer list

Gene	Symbol	Primer 5'-3' Forward	Reverse
Interleukin 6	*Il6*	TTG GTC CTT AGC CAC TCC TTC	TTG GTC CTT AGC CAC TCC TTC
Natriuretic peptide type A	*Nppa*	GCT TCC AGG CCA TAT TGG AG	GGG GGC ATG ACC TCA TCT T
Natriuretic peptide type B	*Nppb*	GAG GTC ACT CCT ATC CTC TGG	GCC ATT TCC TCC GAC TTT TCT C
Myosin, heavy polypeptide 6, cardiac muscle, alpha	*Myh6*	GCC CAG TAC CTC CGA AAG TC	GCC TTA ACA TAC TCC TCC TTG TC
Tumor necrosis factor alpha	*Tnfα*	GAG AGT GGT CAG GTT GCC TC	GCA CCT CAG GGA AGA ATC TGG
Transforming growth factor beta 1	*Tgfβ1*	CAG GAC CTG AGG ACT CCA GA	GGA ATA GGG GCG TCT GAG GA
Transforming growth factor beta 2	*Tgfβ2*	CGA GGA GTA CTA CGC CAA GG	GGA TGG CAT TTT CGG AGG GG
Myosin, heavy polypeptide 7, cardiac muscle, beta	*Myh7*	GTG CCC GAT GAC AAA GAA GAG TTT G	CTT GCC ATT CTC CGT CTC AGC
Interferon-induced protein with tetratricopeptide repeats 2	*Ifit2*	GAG TAC AAC GAG TAA GGA GTC ACT GG	CAT CCT TGT TAA ACA CCC TGT CCT C
Interferon-induced protein 44	*Ifi44*	CTG GAG GCA TTC CAT GGA GTC TTT G	GAG GAT CAG CAT GTC CTT CAC G
Interleukin 1 beta	*Il1β*	CTG CAG CTG GAG AGT GTG G	GGG GAA CTC TGC AGA CTC AA
Chemokine (C-X-C-motif) ligand 10	*Cxcl10*	CAA GTG CTG CCG TCA TTT TCT G	GAT ATG GAT GCA GTT GCA GCG G
ISG15 ubiquitin-like modifier	*Isg15*	CAG TGC TCC AGG ACG GTC TTA C	CTT TCG TTC CTC ACC AGG ATG C
Collagen type 1 alpha 1	*Col1a1*	CCT GTG TGT TCC CTA CTC AGC	GGA ATC CAT CGG TCA TGC TCT C
Collagen type 1 alpha 2	*Col1a2*	GGA GGG AAC GGT CCA CGA TTG	GAG TCC GCG TAT CCA CAA AGC
Collagen type 3 alpha 1	*Col3a1*	GAA GGC GAA TTC AAG GCT GAA GG	GGG TAG TCT CAT TGC CTT GCG T
Hydroxymethylbilane synthase (Ref gene)	*Hmbs*	GGG TGA TTC GAG TGG GCA C	CTC CCG TGG TGG ACA TAG CA
18s ribosomal RNA (Small ribosomal subunit component) (Ref gene)	*18s*	GTA ACC CGT TGA ACC CCA TT	CCA TCC AAT CGG TAG TAG CG

2.8 Histological analysis

For histological staining, formalin-fixed paraffin-embedded (FFPE) midventricular heart tissue was cut with a rotation microtome into 2µm slices. Haematoxylin-eosin staining was performed with decreasing ethanol series, haematoxylin (provided by the Core Facility Imaging, Centre for Medical Research Graz, Austria), eosin (provided by the Core Facility Imaging, Centre for Medical Research Graz, Austria), and increasing ethanol series (protocol paragraph 8.1 page 44) (84) .

Trichrome staining was performed at the Diagnostic and Research Institute of Pathology. Pictures were taken by the BBMRI (Biobanking and BioMolecular Resources Research Infrastructure Austria) and provided via the CaseViewer software from 3DHISTECH. Fibrosis quantification using the trichrome images was analysed using ImageJ software after saturation was increased with GIMP 2.10 software (84) .

2.9 Fluorescence staining

Slices from 2µm thickness, cut with a rotation microtome from FFPEs, were deparaffinised and rehydrated. Antigen retrieval using sodium citrate + 0.05% Tween 20 at a pH6 was performed. Wheat germ agglutination (WGA) fluorescence staining was conducted with a 1:200 dilution for one hour at room temperature. Slices were covered using GLC mounting medium drying for 24 hours at room temperature (protocol paragraph 8.2, page 44) (84) .

Images were taken using the Olympus BX51 fluorescence microscope with a CY3 filter (513 – 556 nm). These were analysed using 20x magnified pictures and the ImageJ software. Four orthogonal spots of every slice have been analysed with the function of 'analyse particles' with a size of 100 – 550 µm² and a circularity of 0.25 – 1.00 (84) .

2.10 Statistical analysis

All data were shown in mean ± standard error of the mean (SEM) normalised to the control and Sham control groups, respectively. Outliers were identified using the ROUT method with a Q=1%. Analysis of more than two groups was performed with two-way ANOVA in case of normality, otherwise Kruskal-Wallis-Test, both with a Bonferroni post hoc test for multiple comparisons. Comparing two groups with normal distribution, Student's tTest was used in all other Mann-Whitney-U-Test. Statistical significance was set at $p \leq 0.05$. All analyses were performed with the GraphPad Prism 8 software (84) .

3 Results

3.1 STING-inhibitor C-178 in permanent myocardial infarction model

For survival analysis of the STING inhibitor C-178, 24 mice were operated on with the permanent ligation model. Twenty mice survived the procedure, leaving ten mice in each group for this experiment. Daily i.p. injections of treatment or control substance were administered for a maximum of 24 days. Using STING inhibitor C-178 showed no effect on myocardial infarction survival (**Fig. 3**) (84) .

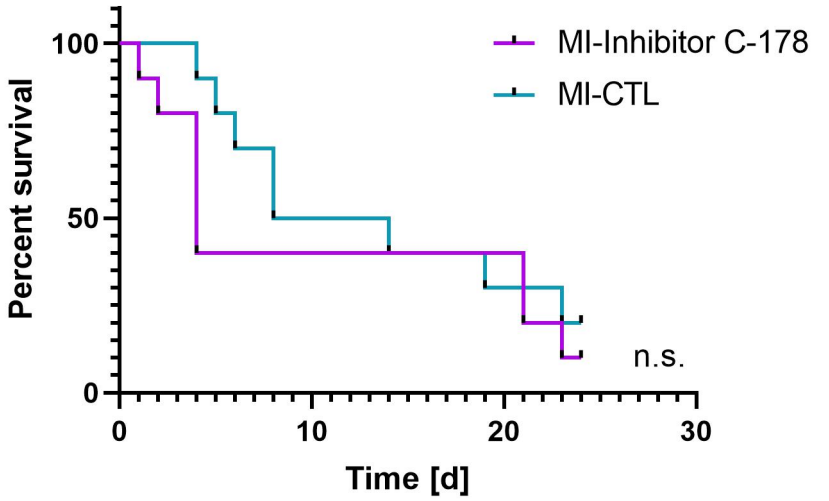

Figure 3: Survival curve permanent ligation
Reproduced from Rech ,L et al Life Sci, 2022(291):120263 with permission under CC BY 4.0 (84)

Another set of 15 mice was operated on with the permanent ligation model for the observation time of 4 days. Six died during the operation procedure, and one during the direct post-op phase. After operation day, eight mice per group were available for further investigation. In total, 9 survived the experimental time of 4 days. Additionally, the MI induction was unsuccessful in one mouse of the MI-Inhib group. In one MI-CTL mouse, infarct zone tissue was not available for qPCR anymore. This left in the infarct zone 3 mice in the MI-CTL and four mice in the MI-Inhib group; further, in the remote zone 4 in the MI-CTL group and 5 in the MI-Inhib group. Structural genes like *Myh6*, *Myh7*, their ratio (*Myh6/Myh7*), and heart failure markers *Nppa* and *Nppb* showed no significant differences between the MI-CTL and the MI-Inhib group, whether in the infarct zone nor the remote zone (**Fig. 4 + 5**).

Additionally, expression levels of the inflammatory markers *Il1β, Il6, Tnfα, Tgfβ1* or *Tgfβ2*, and markers of type I IFN-induced genes like *Ifit2, Ifi44, Cxcl10* and *Isg15* did not display any significant differences (**Fig. 6 - 9**) (84) . Not shown in the figures are outliers, which were excluded from analysis and visualisation.

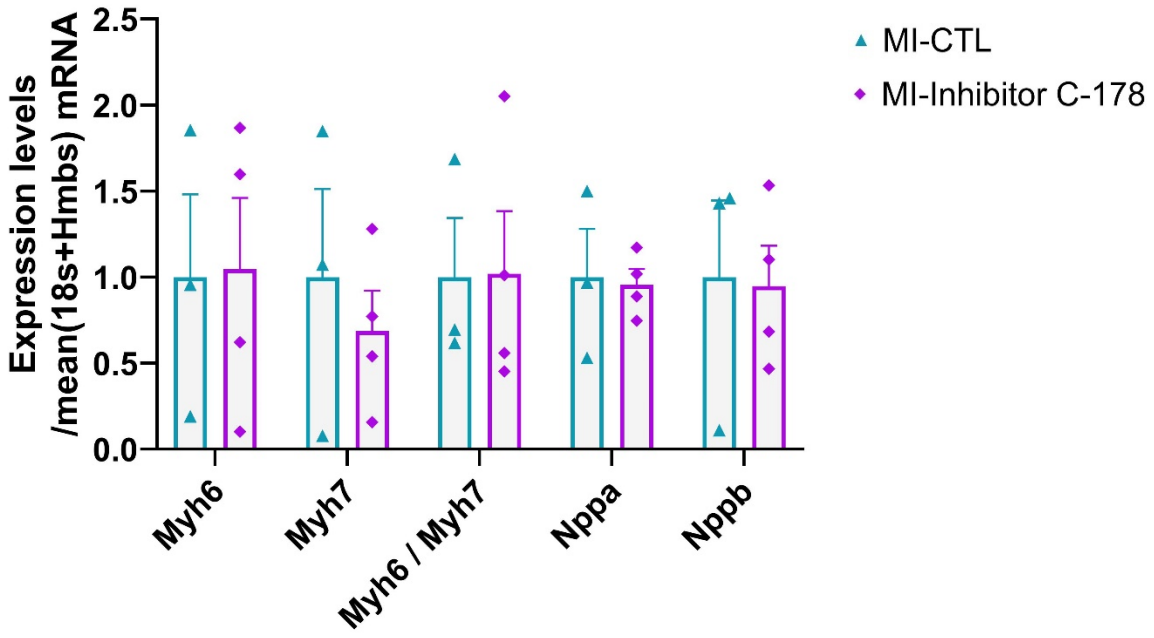

Figure 4: Gene expression in infarct zone - Myh6, Myh6, Myh6/Myh7, Nppa and Nppb; 4 days after permanent ligation

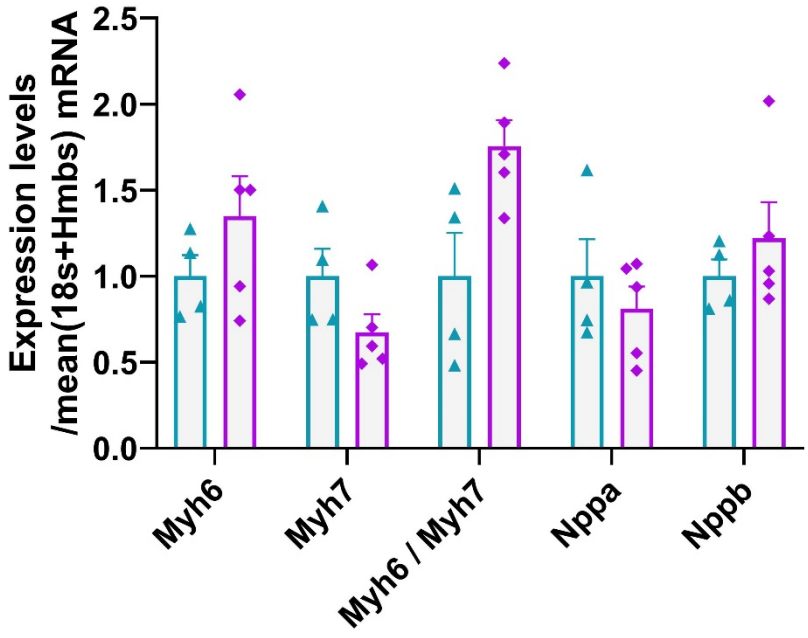

Figure 5: Gene expression in remote zone - Myh6, Myh6, Myh6/Myh7, Nppa and Nppb; 4 days after permanent ligation

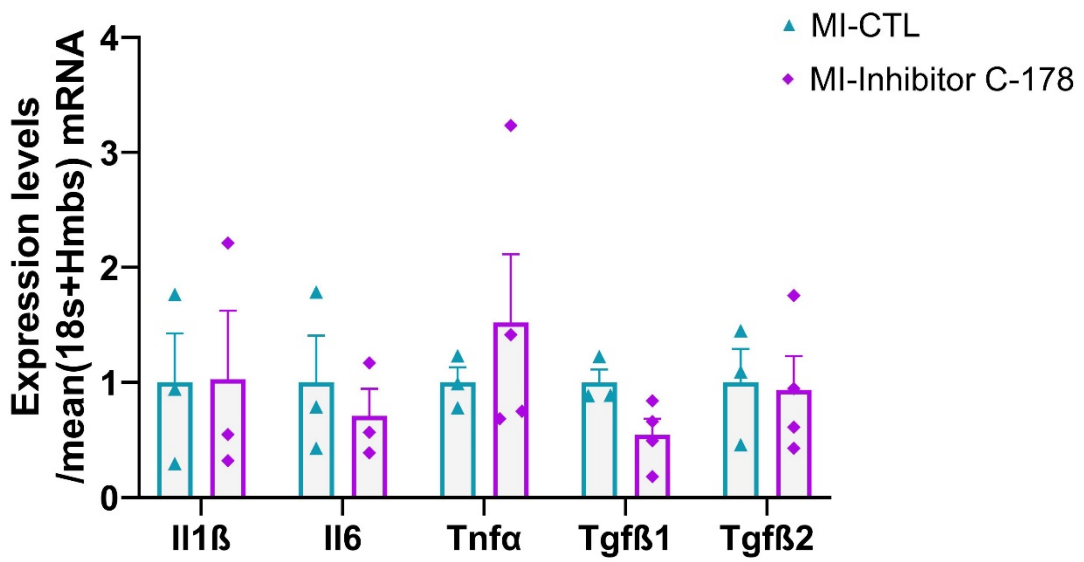

Figure 6: Gene expression in infarct zone - Il1β, Il6, Tnfα, Tgfβ1 and Tgfβ2; 4 days after permanent ligation Reproduced from Rech ,L et al Life Sci, 2022(291):120263 with permission under CC BY 4.0 (84)

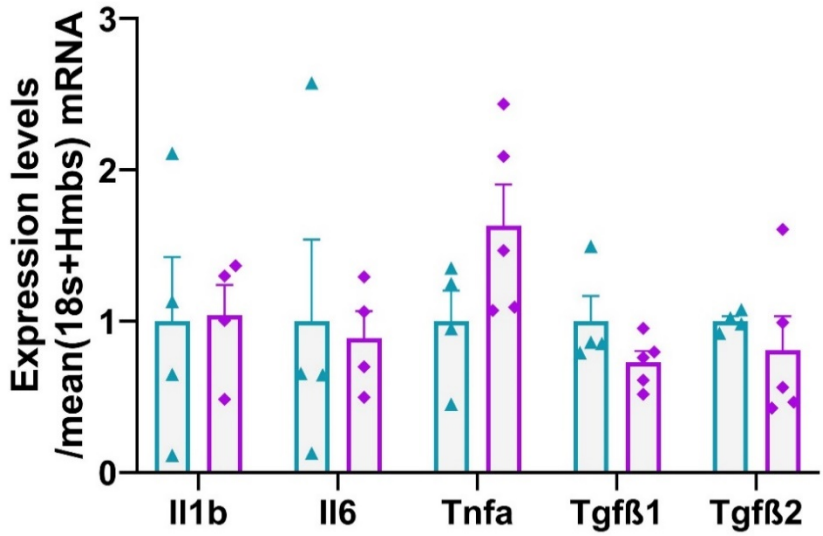

Figure 7: Gene expression in remote zone - Il1β, Il6, Tnfα, Tgfβ1 and Tgfβ2; 4 days after permanent ligation

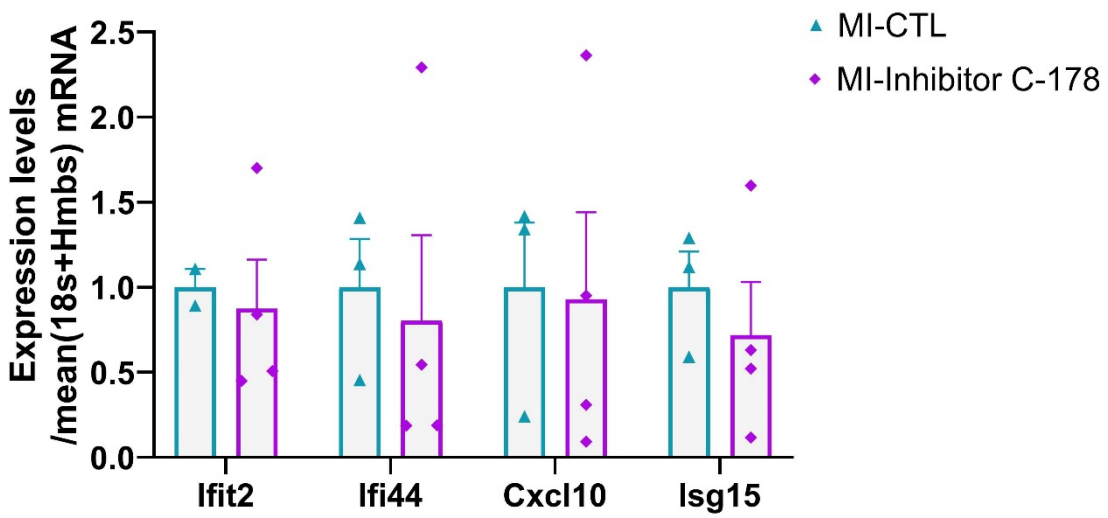

Figure 8: Gene expression in infarct zone - Ifit2, Ifi44, Cxcl10 and Isg15; 4 days after permanent ligation

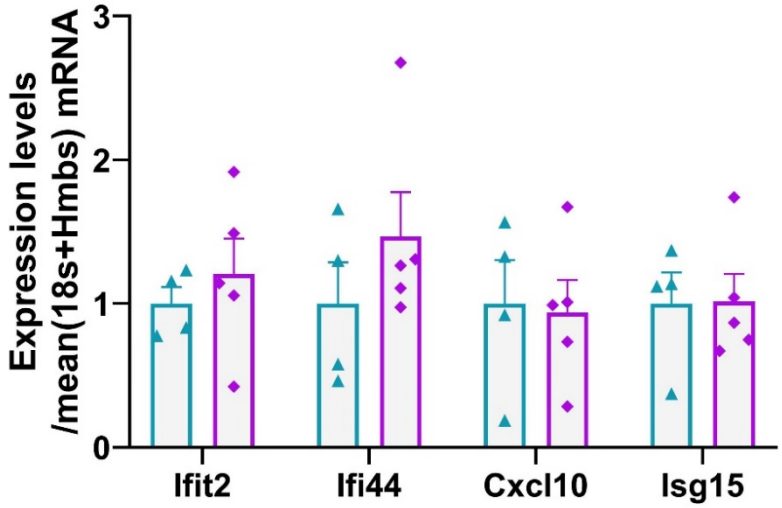

Figure 9: Gene expression in remote zone - Ifit2, Ifi44, Cxcl10 and Isg15; 4 days after permanent ligation

3.2 STING-inhibitor H-151 in reperfused myocardial infarction model

Further experiments used the H-151 STING inhibitor in the ischemic-reperfusion (I/R) model with 30 minutes of ligation. This resulted from the solution problem and the high mortality rate in the permanent ligation model. Additionally, the I/R model is more translational because occluded vessels are reopened in most infarct patients. (84)

3.2.1 Molecular analysis after seven days

In a cohort of mice with an observation time of 7 days, expression levels in the remote zone of the hearts were analysed (no infarct zone tissue was available for this analysis). One mouse died during the operation, leaving 12 mice surviving until the end of this experiment, six in each group. In the expression level of *Il1β*, a significant reduction in the inhibitor group was given (*p = 0.024). The rest of the structural genes (*Myh6, Myh7, Myh6/Myh7, Nppa, Nppb*), including *Col1a1, Col1a2* and *Col3a1*, and the inflammatory genes (*Il6, Tnfα, Tgfβ, Tgfβ2, Ifit2, Ifi44, Cxcl10, Isg15*), did not show any significant differences (**Fig. 10 + 11**). Not shown in the figures are outliers, which were excluded from analysis and visualisation.

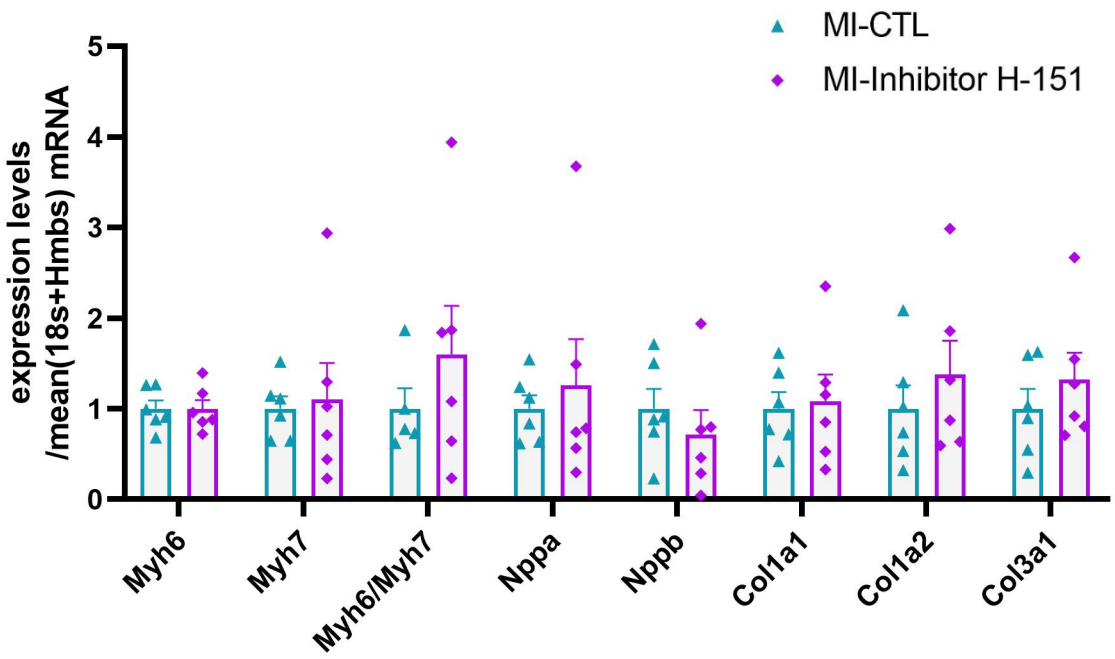

Figure 10: Gene expression in remote zone - Myh6, Myh7, Myh6/Myh7, Nppa, Nppb, Col1a1, Col1a2 and Col3a1; 7 days after ischemic/reperfusion

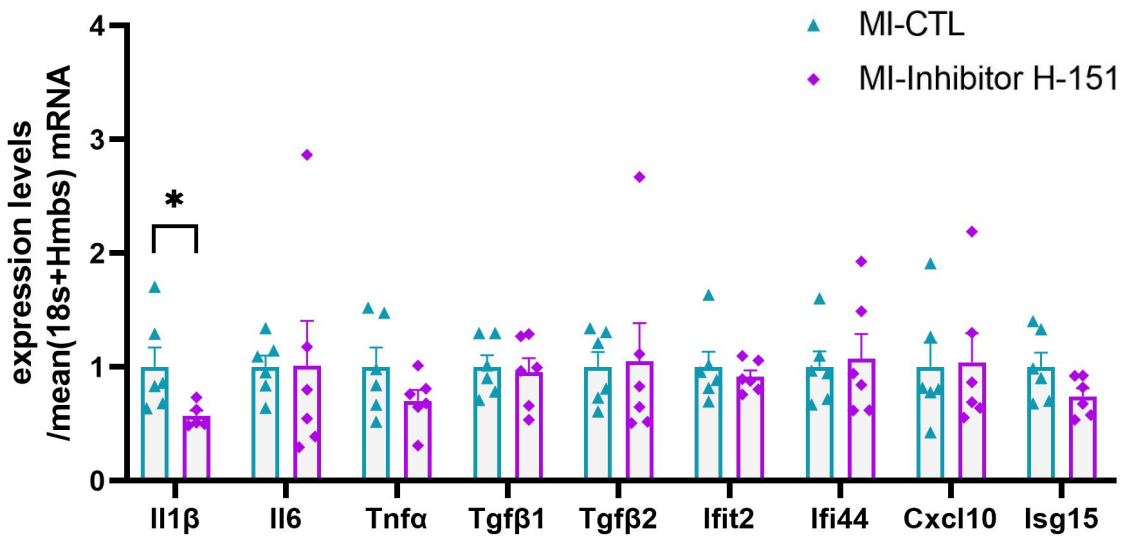

Figure 11: Gene expression in remote zone - Il1β, Il6, Tnfα, Tgfβ, Tgfβ2, Ifit2, Ifi44, Cxcl10 and Isg15; 7 days after ischemic/reperfusion

3.2.2 Phenotypic characterisation

3.2.2.1 Infarct size and echocardiographic assessment

Phenotypic characterisation of the effect of the STING inhibitor on the infarcted heart was done in another cohort. Therefore, the four groups, MI-Inhib, MI-CTL, Sham-Inhib and Sham-CTL, were analysed. Four mice were excluded from the echocardiographic analysis because they displayed a heart with permanent LAD occlusion based on operation complications. This left 11 mice in each group for the MI procedure and 5 mice in each group for the sham operation. Baseline echocardiographic showed no significant differences between all these groups in the endocardial systolic fractional area change (FAC) (**Fig. 14 + 15, Tab. 4**). One day after the operation, both MI groups displayed a significant difference from the sham groups (**Fig. 14§**). At the same time, there was no difference in FAC between the sham groups or between the MI groups (**Fig. 14+15, Tab. 4**) (84) .

The area at risk (AAR) and infarct size on day 1 post-operative were the same in the MI-Inhib group compared to the MI-CTL group (further n=4 per group) (**Fig. 12 + 13**) (84) .

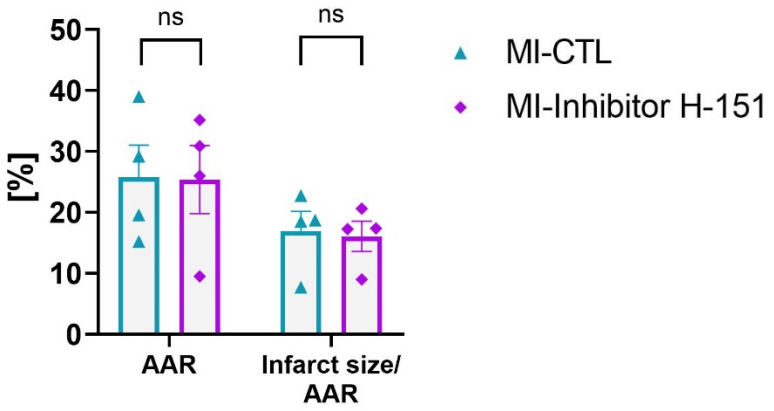

Figure 12: Quantification of area at risk (AAR) and infarct size
Reproduced from Rech ,L et al Life Sci, 2022(291):120263 with permission under CC BY 4.0 (84)

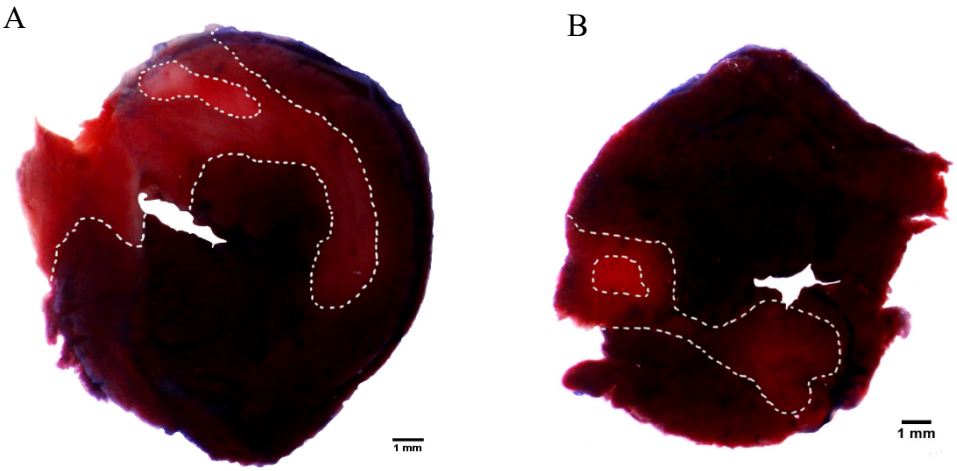

Figure 13: Infarct size representative images (infarct white, area at risk red, normal perfused dark red/blue) at day 1 (A) MI-CTL (B) MI-Inhib
Reproduced from Rech ,L et al Life Sci, 2022(291):120263 with permission under CC BY 4.0 (84)

After three weeks of daily treatment, the MI-Inhib group increased in FAC significantly compared to the MI-CTL group (*p = 0.045). Furthermore, the MI-Inhib group showed no significant difference from the Sham-Inhib group (**Fig. 14 - 16, Tab. 4**) anymore (84) .

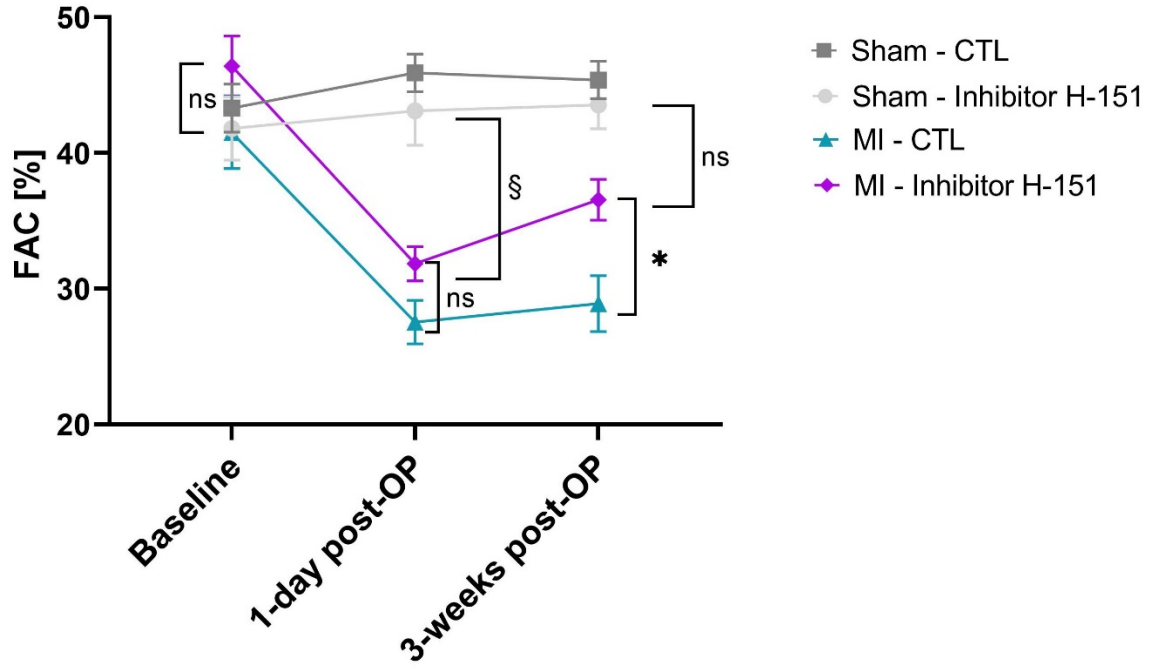

Figure 14: Left ventricular function assessed by endocardial systolic fractional area change (FAC) Reproduced from Rech ,L et al Life Sci, 2022(291):120263 with permission under CC BY 4.0 (84)

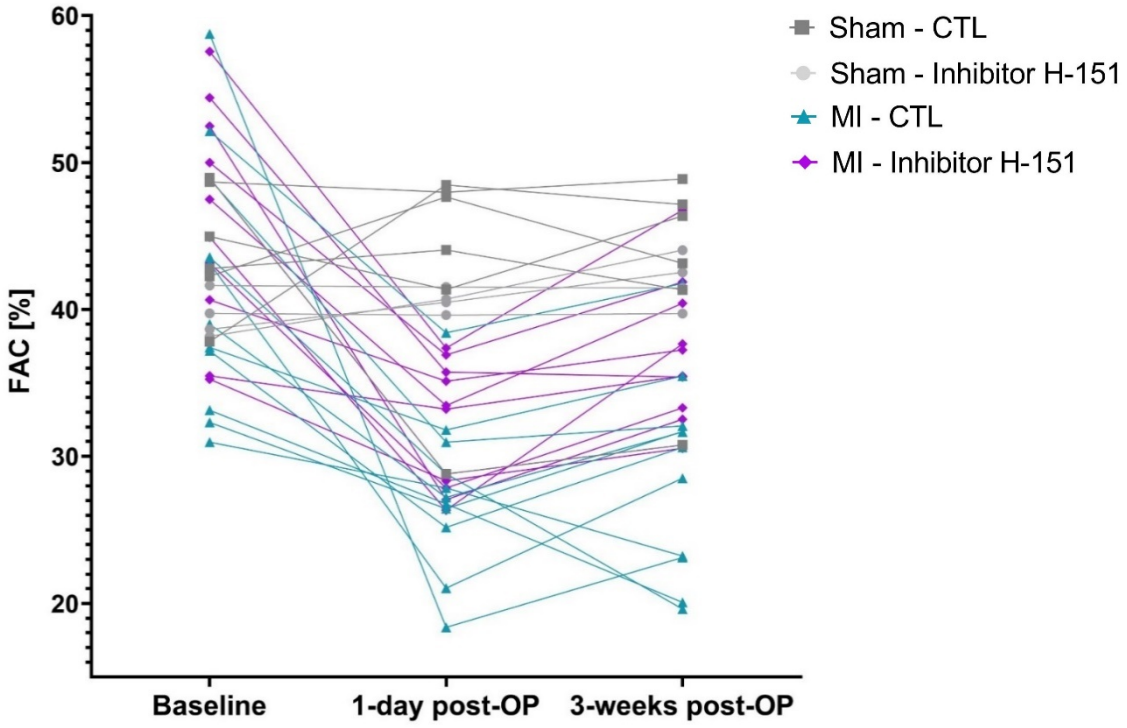

Figure 15: Left ventricular function assessed by endocardial systolic fractional area change (FAC) - individual FAC trajectories
Reproduced from Rech ,L et al Life Sci, 2022(291):120263 with permission under CC BY 4.0 (84)

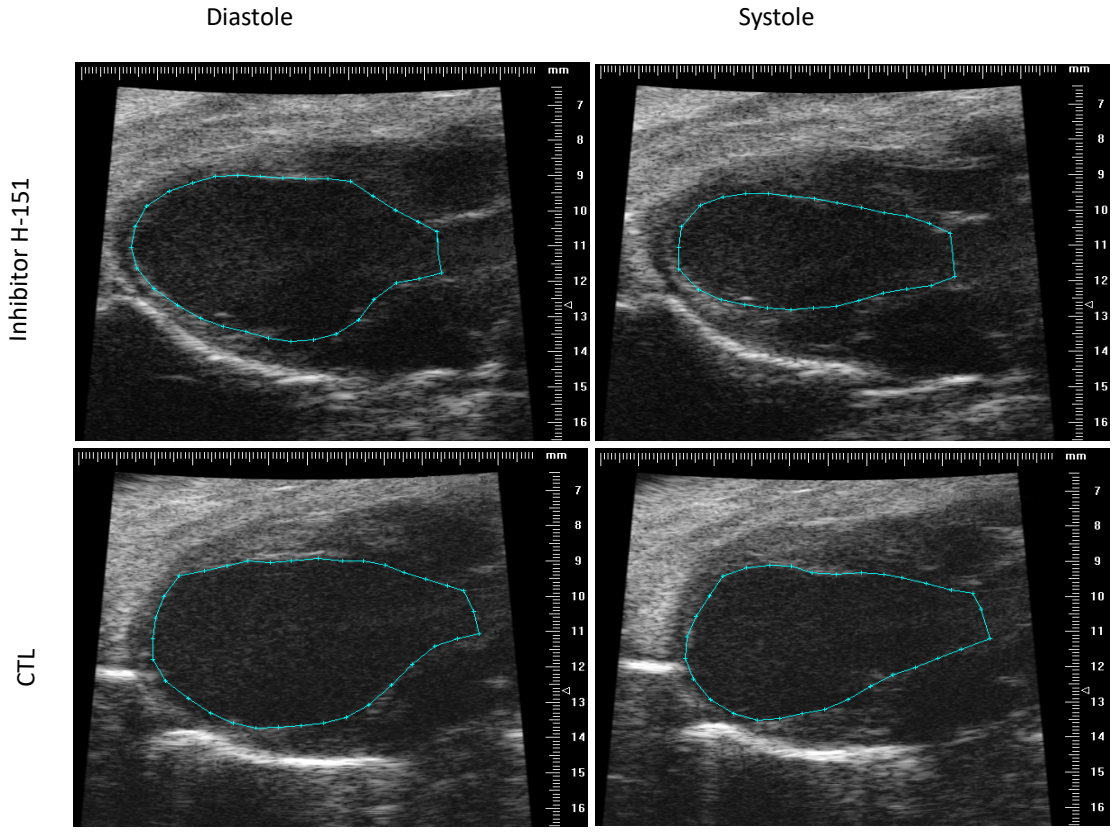

Figure 16: Representative echocardiograms in parasternal long axis view after 3 weeks
Reproduced from Rech ,L et al Life Sci, 2022(291):120263 with permission under CC BY 4.0 (84)

Additional parameters with significant differences in echocardiography due to treatment are the endocardial systolic area (ESA), the left ventricular inner diameter in systole (LVIDs) and diastole (LVIDd) and the posterior wall in diastole (PWd) (**Tab. 4**). Measurements of the LVIDs were done accordingly to the state-of-the-art between a plane mid-ventricular and the valve plane. As the infarct is more related to the apex due to the I/R model (less massive and less severe), additional measurements were performed in a plane more to the apex.

Heart rates during these measurements were not significantly different between the time points and between the groups (**Fig. 17**) (84) . Some more mice in the MI-CTL group showed less than 500 beats per minute compared to one in the MI-Inhib group. Because of this, a linear regression was calculated, indicating that the MI-Inhib group exhibited a higher FAC across different HR levels for the 3-week timepoint (**Fig. 18**).

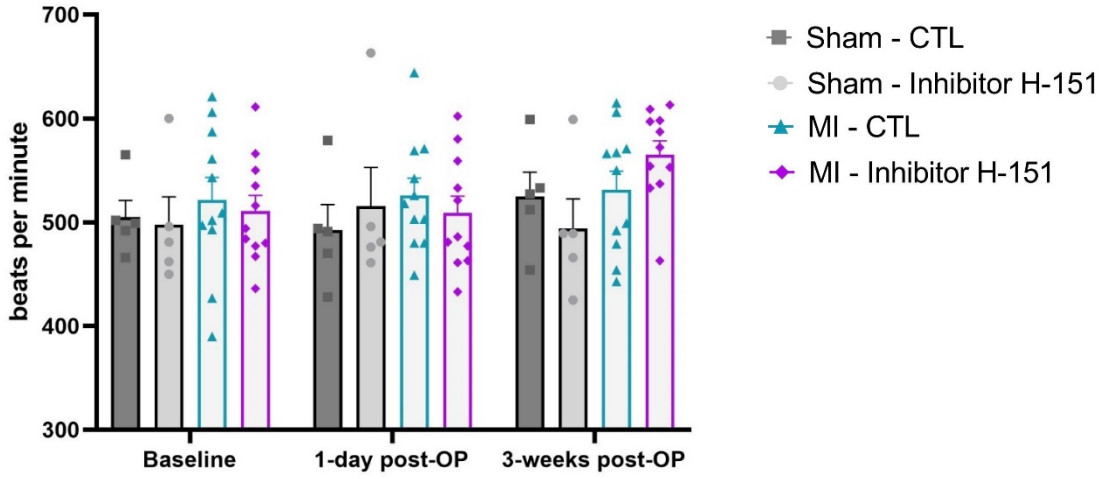

Figure 17: Heart rate during echocardiography

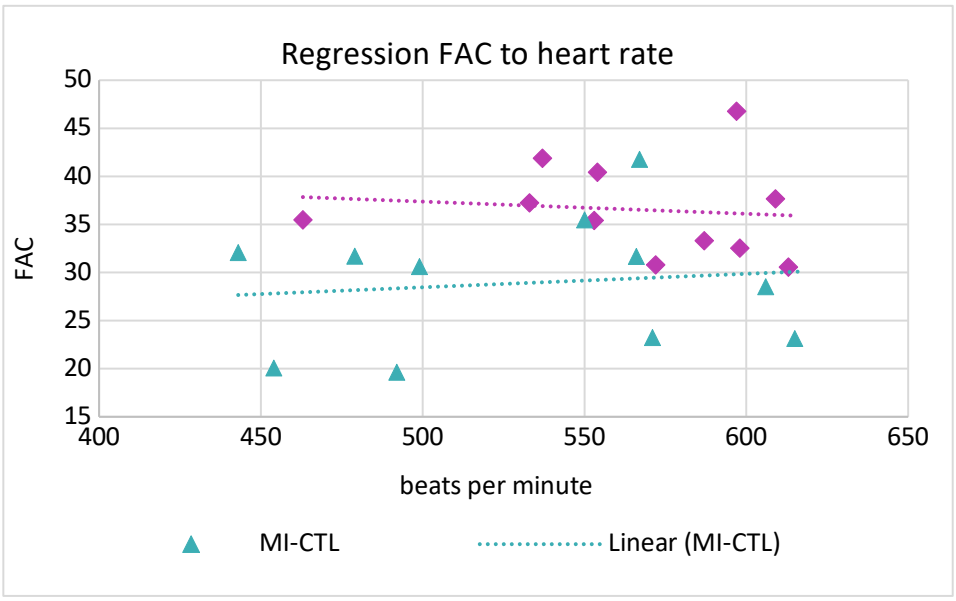

Figure 18: Regression of FAC to heart rate in MI groups after 3 weeks

Table 4: Echocardiographic measurements (84)

Mean ± SEM		Sham - CTL	Sham - Inhibitor H-151	MI - CTL	MI - Inhibitor H-151	two-way ANOVA		
						Interaction	Treatment	Timepoint
Heart rate [beats per min]	baseline	505 ± 16	498 ± 27	522 ± 22	511 ± 15	ns	ns	ns
	1 day post-OP	492 ± 25	515 ± 37	526 ± 16	509 ± 16			
	3 weeks post-OP	525 ± 23	494 ± 29	531 ± 18	565 ± 13			
Endocardial area diastole [mm²]	baseline	22.73 ± 0.96	24.39 ± 1.76	21.50 ± 1.46	22.46 ± 0.58	ns	ns	ns
	1 day post-OP	23.87 ± 0.87	22.50 ± 1.25	24.01 ± 0.75	22.97 ± 0.66			
	3 weeks post-OP	20.51 ± 1.29	22.90 ± 1.16	24.87 ± 0.79	22.59 ± 0.65			
Endocardial area systole [mm²]	baseline	12.89 ± 0.82	14.37 ± 1.48	12.18 ± 1.20	12.06 ± 0.61	0.0029	0.0011	0.0322
	1 day post-OP	13.26 ± 0.41	12.60 ± 1.12	17.41 ± 0.68	15.72 ± 0.70			
	3 weeks post-OP	11.69 ± 0.34	12.82 ± 0.88	17.37 ± 1.09	14.40 ± 0.59			
Endocardial area fractional change (FAC) [%]	baseline	43.30 ± 1.78	41.80 ± 2.32	41.50 ± 2.66	46.40 ± 2.21	0.0004	0.0002	0.0002
	1 day post-OP	45.91 ± 1.38	43.11 ± 2.54	27.54 ± 1.61	31.84 ± 1.27			
	3 weeks post-OP	45.37 ± 1.37	43.54 ± 1.75	28.90 ± 2.06	36.55 ± 1.50			
Left ventricular inner diameter diastole [mm]	baseline	3.679 ± 0.115	3.990 ± 0.257	3.682 ± 0.132	3.687 ± 0.089	0.0275	0.0280	ns
	1 day post-OP	3.837 ± 0.129	3.784 ± 0.213	3.958 ± 0.093	3.743 ± 0.063			
	3 weeks post-OP	3.334 ± 0.066	3.773 ± 0.101	4.105 ± 0.101	3.813 ± 0.092			
Left ventricular inner diameter systole [mm]	baseline	2.235 ± 0.101	2.556 ± 0.243	2.291 ± 0.169	2.165 ± 0.112	0.0043 / 0.0183 (apex/basis)	0.0276 / 0.0002 (apex/basis)	< 0.0001 / 0.0006 (apex/basis)
	1 day post-OP	2.343 ± 0.136	2.255 ± 0.163	3.084 ± 0.156	2.644 ± 0.109			
	3 weeks post-OP apex	1.770 ± 0.040	1.926 ± 0.091	2.958 ± 0.220	2.403 ± 0.127			
	3 weeks post-OP base	1.681 ± 0.128	1.959 ± 0.105	2.473 ± 0.158	2.248 ± 0.093			
Posterior wall diastole [mm]	baseline	0.863 ± 0.039	0.702 ± 0.022	0.855 ± 0.041	0.861 ± 0.037	ns	0.0013	0.0169
	1 day post-OP	0.873 ± 0.056	0,824 ± 0.027	0.909 ± 0.036	0.960 ± 0.035			
	3 weeks post-OP	0.999 ± 0.087	0.810 ± 0.020	0.870 ± 0.032	0.970 ± 0.046			
Posterior wall systole [mm]	baseline	1.415 ± 0.068	1.342 ± 0.073	1.363 ± 0.059	1.464 ± 0.065	ns	ns	0.0358
	1 day post-OP	1.333 ± 0.067	1.334 ± 0.084	1.140 ± 0.070	1.247 ± 0.054			
	3 weeks post-OP	1.102 ± 0.051	1.080 ± 0.037	0.841 ± 0.060	0.900 ± 0.057			

3.2.2.2 Tissue weight and procedure times

Additional measurements displayed no significant differences in body weight (BW), heart weight and left ventricular (LV) weight. Even when the tibia length between the Sham-Inhib group and the MI-Inhib group was significantly different (**Tab. 5**, p = 0.007), others, like the ratio of heart and LV compared to the tibia length, were comparable in all groups (**Tab. 5**). The procedure time (from anaesthesia to extubation) was comparable within the sham or MI groups. In the MI groups, operation time (from the first cut to the last suture) and ligation time were insignificant. All ratios (heart and LV to tibia length and BW) were comparable.

Table 5: Various measurements of time and tissue 3 weeks after ischemic/reperfusion

Mean ± SEM	Sham- CTL	Sham - Inhibitor H-151	MI - CTL	MI – Inhibitor H-151
Procedure time [min]	00:27:00	00:21:15	00:54:55	00:54:55
Procedure time without ligation time[min]	00:27:00	00:21:15	00:23:44	00:25:06
Operation time [min]			00:41:59	00:41:24
Ligation [min]			00:31:11	00:29:49
weight (BW) [g]	28.16 ± 1.51	28.04 ± 1.77	28.50 ± 1.05	28.32 ± 1.34
tibia [mm]	17.52 ± 0.51	17.02 ± 0.35*	17.60 ± 0.36	17.76 ± 0.35*
heart [mg]	130.40 ± 15.66	130.80 ± 13.44	144.40 ± 12.39	141.50 ± 16.05
left ventricle (LV) [mg]	88.60 ± 8.99	89.60 ± 12.28	97.67 ± 12.99	92.45 ± 14.38
heart /BW [mg/g]	4.62 ± 0.38	4.66 ± 0.31	5.07 ± 0.43	4.99 ± 0.44
heart /tibia [mg/mm]	7.43 ± 0.75	7.69 ± 0.80	8.21 ± 0.71	7.97 ± 0.86
LV / BW [mg/g]	3.14 ± 0.20	3.19 ± 0.37	3.43 ± 0.46	3.26 ± 0.40
LV / tibia [mg/mm]	5.05 ± 0.40	5.27 ± 0.75	5.54 ± 0.75	5.21 ± 0.81

* significant difference between MI-Inhib and Sham-Inhib (ANOVA)

3.2.2.3 Histological assessment

The echocardiographical findings were supported by fibrosis and hypertrophy measurements after these three weeks. Fibrosis analysed with Masson Trichrome staining (n = 3) showed a significant reduction of fibrosis of MI-Inhib compared to MI-CTL in the whole heart (*p=0.0129). Further, a more divided analysis was done between the infarct and remote zones. This was necessary to distinguish between the scar in the infarct zone as this is replacement fibrosis compared to intestinal fibrosis in the remote zone. This analysis showed a significant reduction of fibrosis from MI-CTL to MI-Inhib (**p = 0.0010).

At the same time, there were no significant differences in fibrosis between all groups in the remote zone (n = 3) (**Fig. 19 + 21**).

Hypertrophy, measured by WGA staining and analysis of the cardiomyocyte cross-sectional area (CSA) (n =3; >1100 cells on average per n), also displayed a decrease in CSA from MI-CTL to MI-Inhib (**p = 0.0016) (**Fig. 20 + 21**) (84) . While there were no significant differences in the heart weight or heart weight to body weight (HW/BW) between all groups, an increased trend in the MI-groups could be observed. Further, a tTest analysis of MI-CTL to Sham-CTL (HW/BW) led to a p-value of p=0.065, indicating that with a larger sample size, these effects would also be visible in the heart weight. Hypertrophy on the cellular level was already significantly observable because the analysed sections were cut midventricular and, therefore, in the infarct area with more detectable differences.

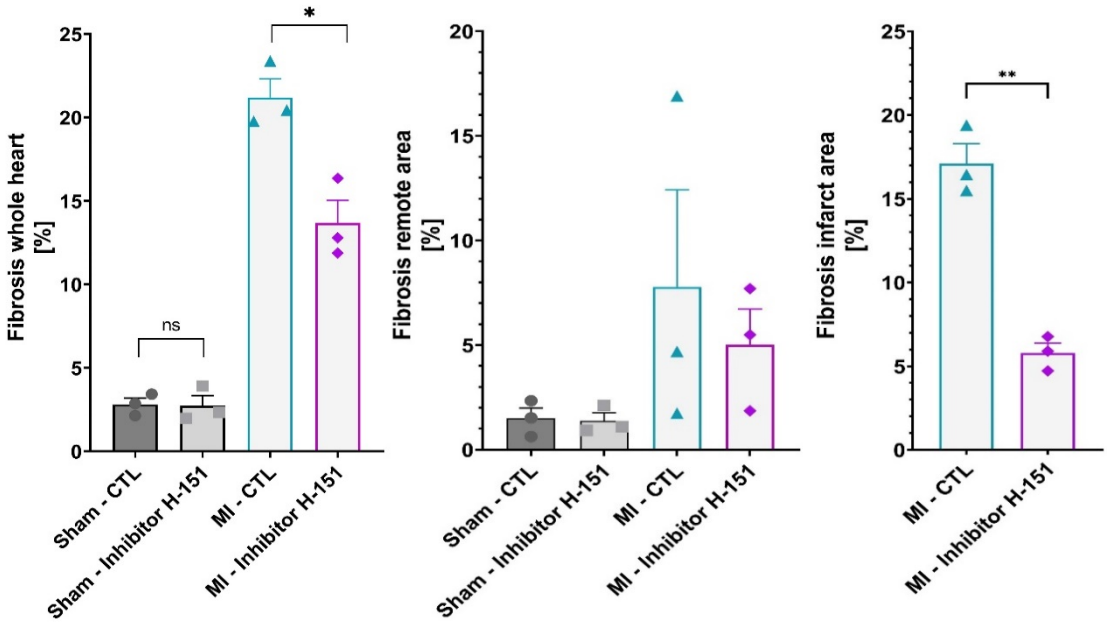

Figure 19: Collagen area fraction
Reproduced from Rech ,L et al Life Sci, 2022(291):120263 with permission under CC BY 4.0 (84)

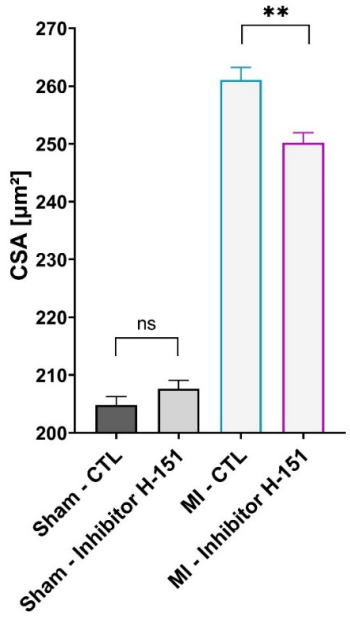

Figure 20: Myocyte cross-sectional area (n=3 hearts per group, >1100 cells per heart) Reproduced from Rech, L et al Life Sci. 2022 (291):120263 with permission under CC BY 4.0 (84)

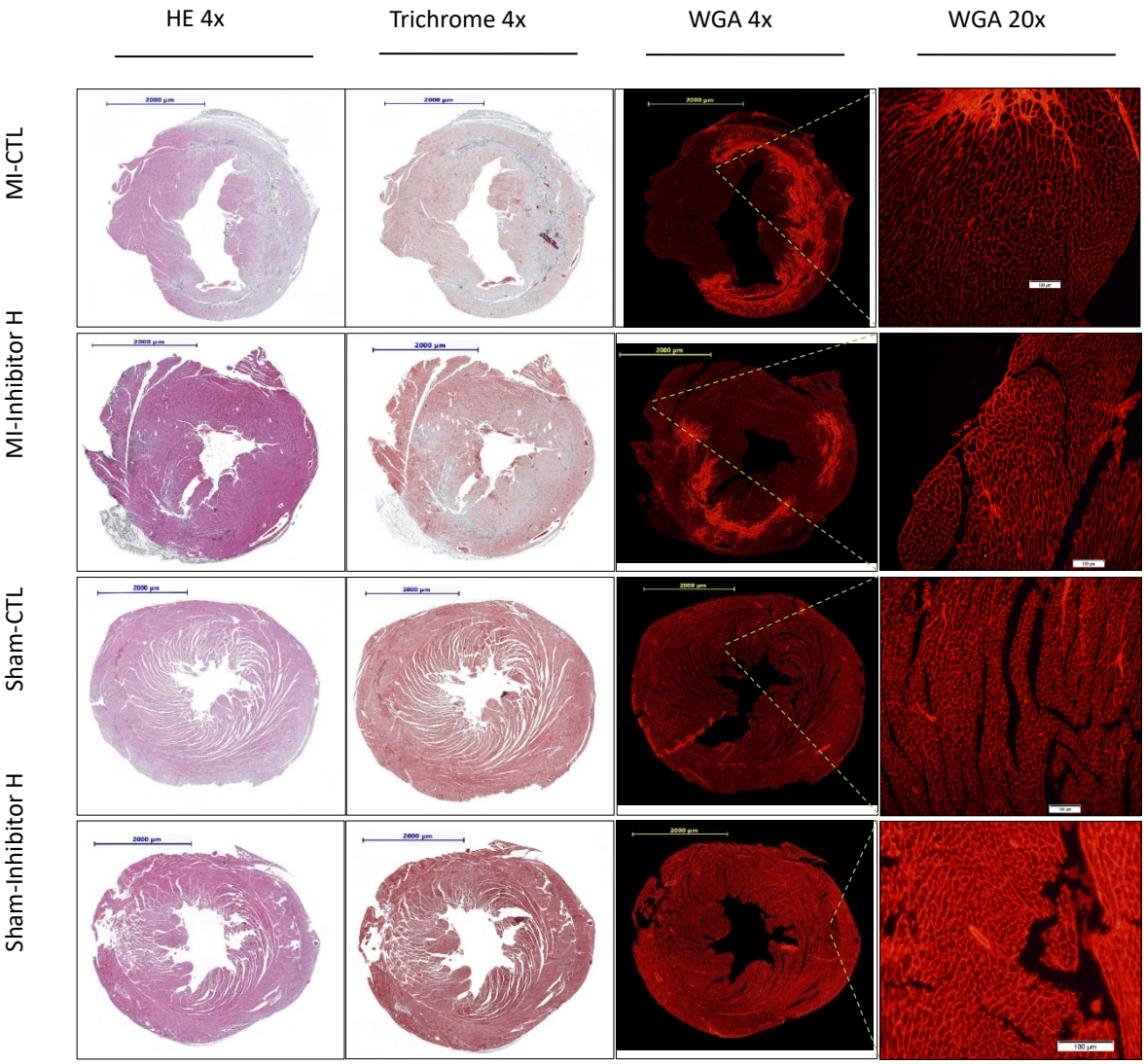

Figure 21: Representative images for HE, Masson Trichrome, and WGA staining. Scale bar 2mm (2000 µm) in 4x; scale bar 100 µm in 20x. Reproduced from Rech ,L et al Life Sci, 2022(291):120263 with permission under CC BY 4.0 (84)

3.2.3 Molecular Analysis after 21 days

Moreover, the expression levels of the above-named structural genes and inflammatory markers in the infarct and the remote zone of the infarcted hearts were analysed. For analysis of the remote zone, 8 samples for each MI group and 5 samples in each Sham group were analysed. In the infarct zone, one sample in the MI-CTL group was excluded based on too little RNA in extraction. Furthermore, in the groups of MI-Inhib and Sham-Inhib, one in each was excluded after qPCR based on Ct-values over 35 in all measurements. Individual values were further excluded based on the outlier's analysis.

In the remote zone, just a few changes are visible. Significant increases can be observed in *Nppa* and *Col3a1* from sham-operated to MI mice. These significant variances in the operation type can also be observed in *Col1a2* (##). Furthermore, the ANOVA analysis displays a significant variance in interaction for *Ifit2* and *Isg15* (#) (**Fig. 22** + **23**) (84) .

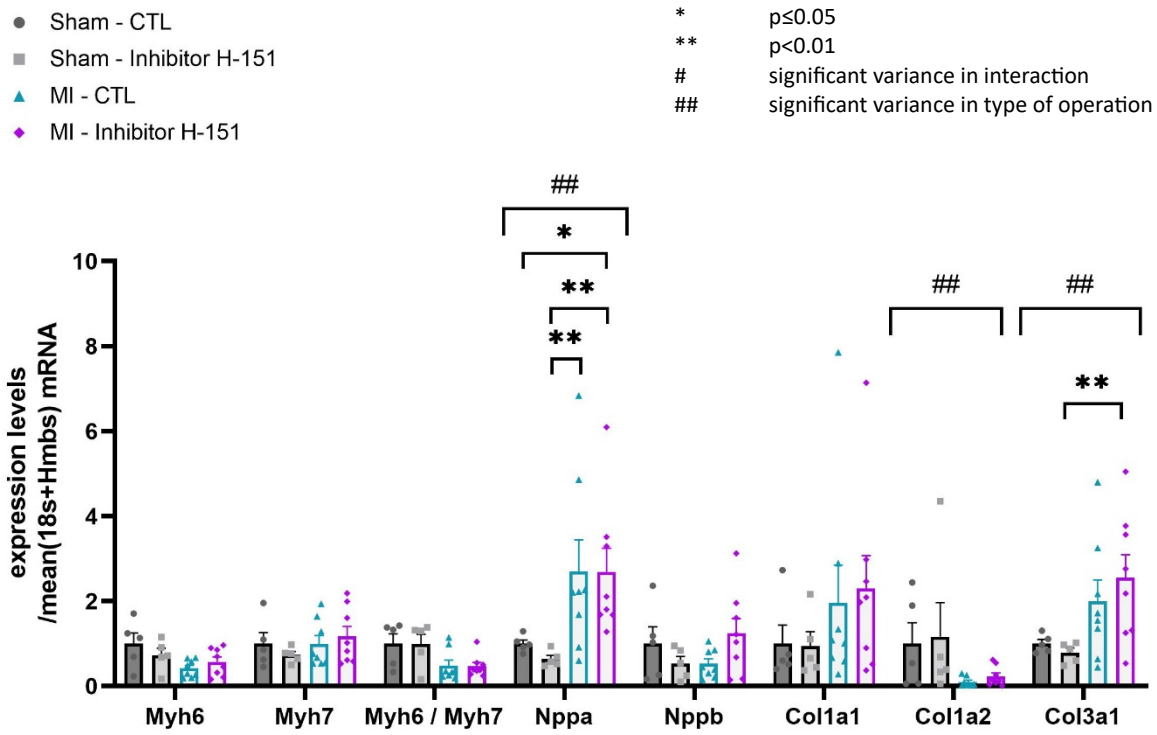

Figure 22: Gene expression in remote zone - Myh6, Myh7, Myh6/Myh7, Nppa, Nppb, Col1a1, Col1a2 and Col3a1; 21 days after ischemic/reperfusion

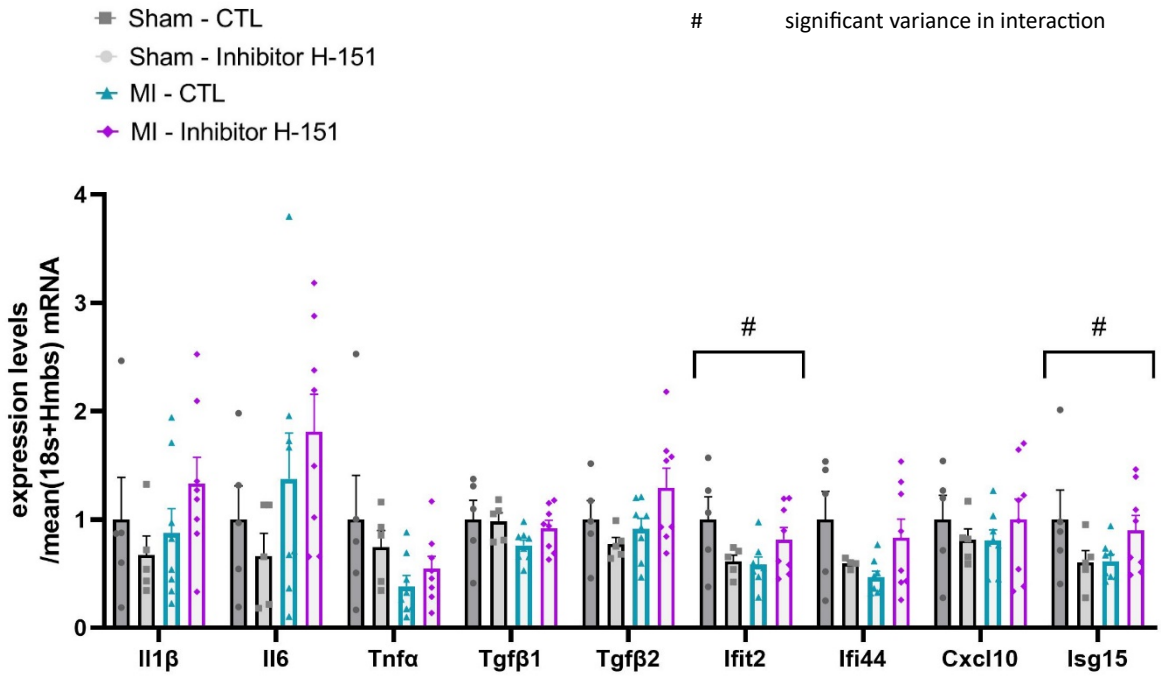

Figure 23: Gene expression in remote zone - Il1β, Il6, Tnfα, Tgfβ1, Tgfβ2, Ifit2, Ifi44, Cxcl10 and Isg15; 21 days after ischemic/reperfusion

In the infarct zone, more changes are visual in the inflammatory markers. Nearly all markers (*Il1b, Il6, Tgfβ2, I fit2, Ifi44, Cxcl10, Isg15*) showed decreasing trends from MI-CTL to MI-Inhib. Furthermore, analysing these two groups separately with students' t-test or Mann-Whitney U to increase power, *Ifi44* and *Cxcl10* showed a significant difference (*p = 0.0249 and *p = 0.0208, respectively). A significant variance in the operation type can be seen in *Il6, Tnfα, Tgfβ1, Tgfβ2, Ifit2, Cxcl10* and *Isg15* (##). Interestingly, in *Tnfα* and *Tgfβ1*, the MI model showed decreased levels compared to the sham-operated. Moreover, in *Tgfβ1*, the treatment of MI mice with the inhibitor increased the levels significantly compared to the MI-CTL group (*p = 0. 0262) (**Fig. 24 - 26**) (84) .

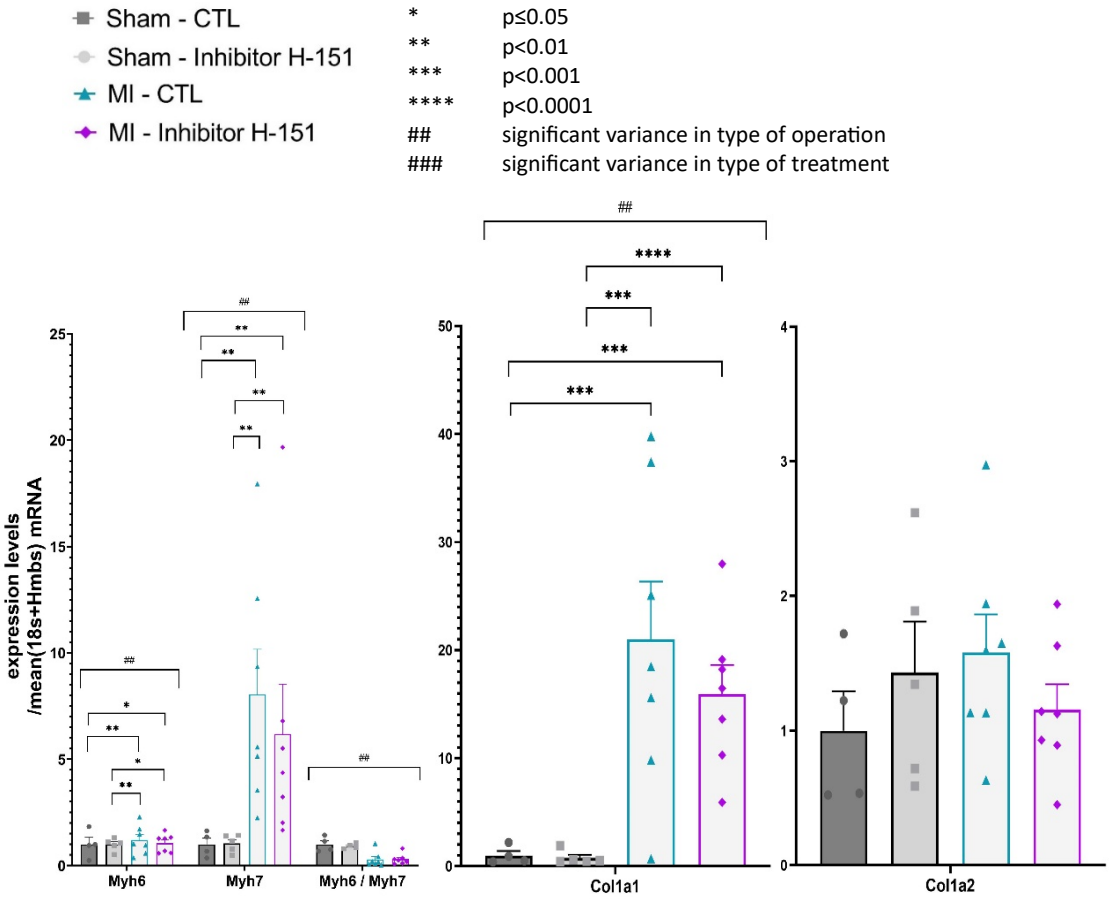

Figure 24: Gene expression infarct zone - Myh6, Myh7, Myh6/Myh7, Col1a1 and Col1a2; 21 days after ischemic/reperfusion
Reproduced from Rech ,L et al Life Sci, 2022(291):120263 with permission under CC BY 4.0 (84)

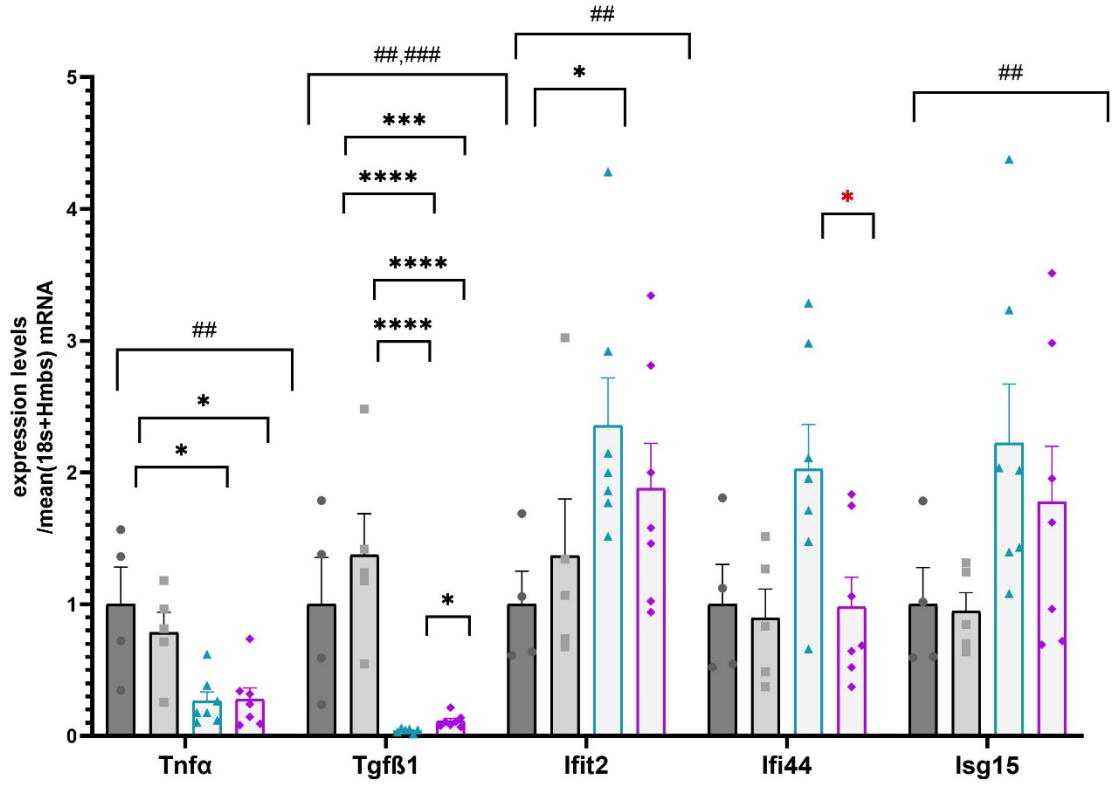

Figure 25: Gene expression infarct zone - Tnfα, Tgfβ1, Ifit2, Ifi44 and Isg15; 21 days after ischemic/reperfusion
Reproduced from Rech ,L et al Life Sci, 2022(291):120263 with permission under CC BY 4.0 (84)

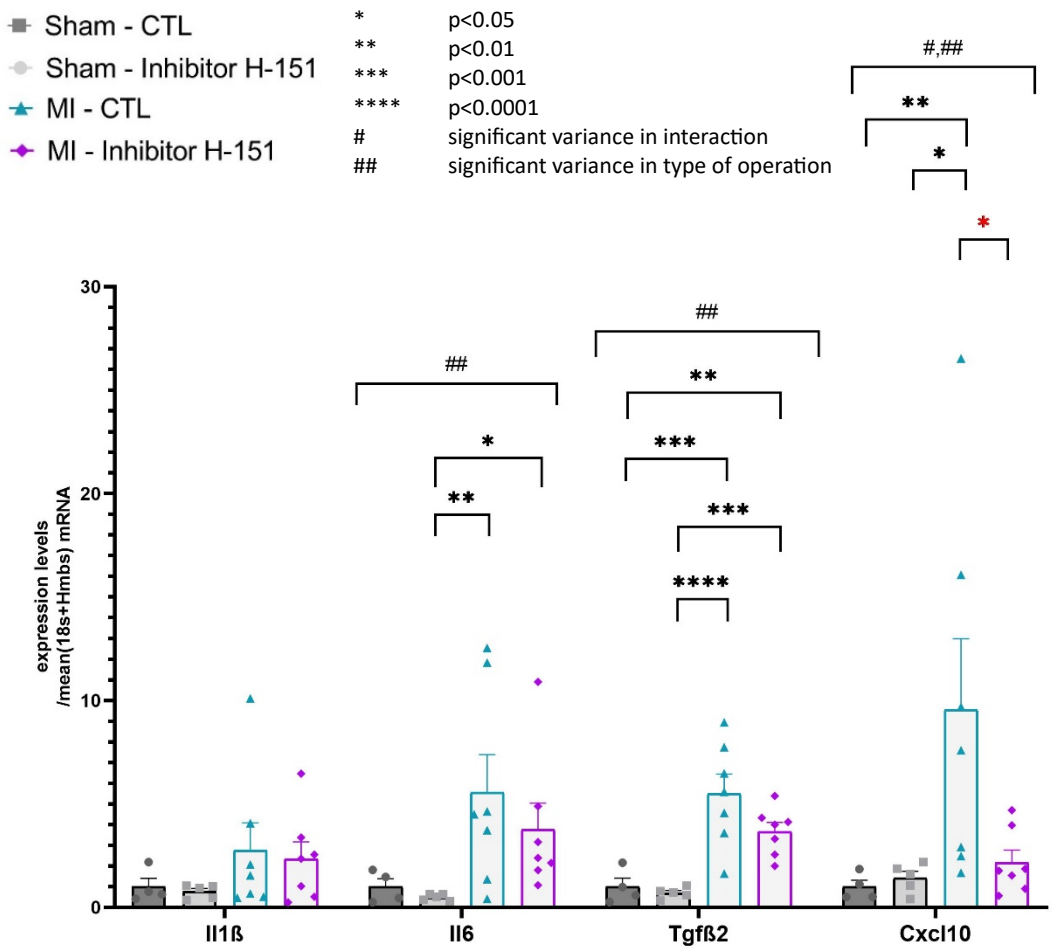

Figure 26: Gene expression infarct zone - Il1β, Il6, Tgfβ2 and Cxcl10; 21 days after ischemic/reperfusion (84)

4 Discussion

Myocardial infarction and its consequences are one of our world's most tremendous burdens. Improving the outcomes is a big challenge and is still under much investigation. Targeting the immune system seems a good approach. One of these targets is the cGAS-STING pathway, activated by non-nuclear DNA and results in a type I IFN response. It is a decent target as non-nuclear DNA could be found in patients suffering from an MI (107), and this leads to an increase in IFN, which is associated with worse cardiac healing (108). The cGAS-STING pathway connects non-nuclear DNA to IFN release in MI. Therefore, we hypothesised that small molecule STING inhibitors reduce the expression levels of IFN-induced chemokines Ifi44, Ifit2, Cxcl10 and Isg15. We aimed to attenuate maladaptive inflammatory remodeling processes after MI to enable efficient healing and prevent ensuing heart failure.

We showed that small molecule STING inhibition successfully improved left ventricular function after MI and reduced IFN-induced genes.

We use the endocardial fractional area change (FAC) for echocardiographic evaluation because the MI model shows better results for assessing the reduced LV function than ejection fraction or fractional shortening in mice (109), with constant stability during the ageing process in healthy mice (84, 110). Echocardiographical measurements in mice are strongly related to the heart rate, which anaesthesia can impair (111). Therefore we compared all heart rates, showing no differences during all time points with adequate rates of around 500 beats per minute (112).

Given this, baseline FAC was insignificant between all four groups. One day post-op, we saw the expected significant decrease in FAC in the MI groups compared to the sham-operated mice. No significant differences could be observed between the MI-Inhib group and MI-CTL. This was confirmed by evaluating both MI groups' AAR and infarct size (84). Even if these sizes are the same in both MI groups, they seem smaller than other groups reported in C57/BL6 mice (113, 114). However, the reperfusion time until the analysis impacts this as well as the operator’s experience (115).

Further, after 3 weeks of daily treatment, we recognised a significant increase in FAC in the MI-Inhib group compared to the MI-CTL mice due to less infarct expansion. Furthermore, there was no longer a significant difference in the Sham-Inhib group anymore (84) . A similar observation with preserved LV ejection fraction (EF) using H-151 showed the paper of Hu et al. after 28 days of daily treatment (100) . Interestingly, King et al. did not see any influence in different echocardiographic parameters in the $STING^{gt/gt}$ mice (99) , suggesting additional pathways could be involved, which were not entirely suppressed by our inhibition.

Our findings of improved cardiac function were affirmed by a significant reduction of fibrosis in the heart of the MI-Inhib group. The reduction was localised dominantly in the infarct zone, meaning a smaller scar (84) . A similar was seen by Hu et al. (100) . However, they could link this to significantly reduced collagen I and III expressions on the molecular level (100) ; we could show just reduction trends of *Col1a1* in the infarct zone (84) . A possible reason for these differences could be the different operation type, I/R in our case and the more severe permanent ligation otherwise. Furthermore, as we saw decreasing trends, a larger sample size could provide a more visible and significant effect.

Further, we set up a cohort for 21 days of treatment after I/R MI and compared them to sham-operated mice on molecular levels. The decreasing expression trends of different type I IFN-induced chemokines supported working inhibition. Unfortunately, these differences are not significant in ANOVA analysis. Only tTests between the MI groups to increase power in analysis displayed significant reductions in *Ifi44* and *Cxcl10*, as Hu et al. could observe after 28 days as well (84, 100) . The different time points of investigation and other access to cardiac remodeling could explain this. In comparison, in the pressure overload model, the peak of *cGAS*, *STING*, *Cxcl10* and *Isg15* were described on day three and were reduced to normal within 7 days (96) .

We could not improve survival in our study, similar to the findings from King et al. with their $STING^{gt/gt}$ mice with MI. However, they showed a higher survival rate for WT and $STING^{gt/gt}$ than ours (84, 99) . Interestingly, the survival rate for the permanent ligation model in C57/BL6 mice ranges from 30 % to 80% (115) . Compared to 14 days of observance, like King et al., we had a survival rate of 40% and 50%, respectively. Unfortunately, another group studying STING inhibition in MI did not show survival curves (100) . In our study reason for no beneficial survival outcome of the treatment could be, on the one hand, the high mortality rate due to ventricular rupture. On the other

hand, it could be due to the small effect and the few mice we investigated. Further, it is plausible that in permanent ligation as a model for a severe infarction, the inhibitor C-178 is not potent enough or not potent in the early process of rupture after MI, only in the later cardiac remodelling.

Another finding from Hu et al. was the increase of αSMA after MI and the partial reduction using H-151 (100) . This is interesting, as αSMA increase is known in endothelial-to-mesenchymal transition (EndMT). EndMT describes in the heart the conversion of endothelial cells into myofibroblasts during oxidation stress (116) . This mechanism is induced via TGFβ (116, 117) . There is evidence that macrophages are the main driver of the EndMT after MI (118) . Myocardial infarction leads to an upregulation of TGFβ (119) . Further, TGFβ activates the expression of SNAIL, which in turn induces the polarisation of macrophages into the M2-type (120) . This would be in accordance with a balanced switch from a pro-inflammatory, M1-dependent phase to the M2-associated pro-reparative phase (25–27) . Another hint for the involvement of STING in EndMT is that Cao et al. saw decreasing STING expression after patients received an LVAD (98) . The implantation of an LVAD could result in a less disturbed flow, which is in atherosclerosis, a known factor for EndMT (121) .

The decreased levels of *Tnfα* in the MI groups compared to the sham groups in our study could be explained by the use of DMSO either, as it is known that DMSO is a suppressor for *Tnfα* (122) . While Sham-operated mice also received DMSO, it could be due to the increased flow because of the inflammatory response that MI-mice consumed a higher DMSO dose in the heart than Sham-operated mice and therefore did not show these decreases in *Tnfα.* Additionally, our study found a significant increase in *Tgfβ1* expression level in the MI-Inhib group compared to the MI-CTL once (84) . A possible explanation would be negative feedback because Tgfβ usually blocks type I IFN and is critical for inflammation suppression (123, 124) . Additionally, this would support the previously mentioned switch from the pro-inflammatory phase to the pro-reparative one. Nevertheless, it is curious that *Tgfβ1* is decreased in the MI groups compared to the Sham groups in contrast to the regular increase after MI, as seen with *Tgfβ2* (119) . Moreover, it contrasts the increased αSMA found by Hu et al. (100) , as it is known that *Tgfβ* induces the expression of *αSMA* (125) .

5 Limitations

Molecular analysis four days after permanent MI with C-178 treatment showed no differences. A possibility for nonsignificance can be the choice of our control substance. As the inhibitor was dissolved in DMSO, we used the same amount as the control. DMSO is also anti-inflammatory (126) . Thus, the effect of the inhibitor itself could be negligible. Lastly, we had dissolving problems with the inhibitor C- 178. Unfortunately, even when DMSO is a good solvent solution, we cannot increase it due to its cardiotoxicity (127) . As a consequence of the solution problem and the high mortality rate in the permanent ligation model, we changed the inhibitor to H-151 and the operation method to the ischemic/reperfusion (I/R) model. The STING inhibitor H-151 has the additional advantage that it works for mouse and human STING (63) and is, therefore, very interesting in a translational approach. Additionally, the I/R model is more translational because occluded vessels are reopened in most infarct patients (84) . However, after 7 days of daily injection, no significance to the treatment was observed in the remote zone after I/R MI on molecular levels (84) . As the remote zone is not the main focus of the hypoxia and the inflammation, we did not expect any differences. Unfortunately, it was not possible to analyse tissue from the infarct zone.

More general limitations include that we did not study the detailed inflammatory and cell-specific response nor the cell types involved in the inhibition process. Further, wound healing after MI is a dynamic process of different phases involving specific timing and duration for the treatment. This is a topic which we did not address either during this thesis. Moreover, the first injection should be given after the operation for the human translational approach after MI. Lastly, we used only male mice, so further studies with female mice need to determine if our findings can be generalised (84) .

6 Conclusion

Our study demonstrated *in-vivo* that targeting this pathway with a STING inhibitor improves the systolic function and reduces infarct size after myocardial infarction. However, this pathway is still our first-line defence against bacteria and viruses. Further investigations are indispensable for the right balance of immune system suppression against worsening the outcome after MI. Nevertheless, this target is worth further investigation for cardiovascular diseases.

Literature

1. Wilkins E, Wilson L, Wickramasinghe K, Bhatnagar P, Leal J, Luengo-Fernandez R, Burns R, Rayner M, Townsend N. European Cardiovascular Disease Statistics 2017. Brussels; 2017.

2. World Health Organisation. Cardiovascular diseases; 2021 [cited 2021 Aug 25]. Available from: URL: https://www.who.int/health-topics/cardiovascular-diseases#tab=tab_1.

3. Townsend N, Kazakiewicz D, Lucy Wright F, Timmis A, Huculeci R, Torbica A et al. Epidemiology of cardiovascular disease in Europe. Nat Rev Cardiol 2022; 19(2):133–43. doi:10.1038/s41569-021-00607-3.

4. Timmis A, Vardas P, Townsend N, Torbica A, Katus H, Smedt D de et al. European Society of Cardiology: cardiovascular disease statistics 2021. European Heart Journal 2022; 43(8):716–99. doi:10.1093/eurheartj/ehab892.

5. Virani SS, Alonso A, Aparicio HJ, Benjamin EJ, Bittencourt MS, Callaway CW et al. Heart Disease and Stroke Statistics-2021 Update: A Report From the American Heart Association. Circulation 2021; 143(8):e254-e743. doi:10.1161/CIR.0000000000000950.

6. Mohammad MA, Persson J, Buccheri S, Odenstedt J, Sarno G, Angerås O et al. Trends in Clinical Practice and Outcomes After Percutaneous Coronary Intervention of Unprotected Left Main Coronary Artery. Journal of the American Heart Association 2022; 11(7):e024040. doi:10.1161/JAHA.121.024040.

7. Jenča D, Melenovský V, Stehlik J, Staněk V, Kettner J, Kautzner J et al. Heart failure after myocardial infarction: incidence and predictors. ESC Heart Fail 2021; 8(1):222–37. doi:10.1002/ehf2.13144.

8. Frangogiannis NG. Regulation of the inflammatory response in cardiac repair. Circulation Research 2012; 110(1). doi:10.1161/CIRCRESAHA.111.243162.

9. Westman PC, Lipinski MJ, Luger D, Waksman R, Bonow RO, Wu E et al. Inflammation as a Driver of Adverse Left Ventricular Remodeling after Acute Myocardial Infarction. Journal of the American College of Cardiology 2016; 67(17):2050–60. doi:10.1016/j.jacc.2016.01.073.

10. Christia P, Frangogiannis NG. Targeting inflammatory pathways in myocardial infarction: NIH Public Access. 00142972; 2013. (vol 43).

11. Frangogiannis NG. The inflammatory response in myocardial injury, repair, and remodelling. Nature Reviews Cardiology 2014; 11(5):255–65. doi:10.1038/nrcardio.2014.28.

12. Swirski FK, Nahrendorf M. Cardioimmunology: the immune system in cardiac homeostasis and disease. Nature Reviews Immunology 2018; 18(12):733–44. doi:10.1038/s41577-018-0065-8.

13. Nahrendorf M, Swirski FK, Aikawa E, Stangenberg L, Wurdinger T, Figueiredo J-L et al. The healing myocardium sequentially mobilizes two monocyte subsets with divergent and complementary functions. The Journal of Experimental Medicine 2007; 204(12):3037–47. doi:10.1084/jem.20070885.

14. Hofmann U, Frantz S. Role of T-cells in myocardial infarction. European Heart Journal; 2016. (vol 37).

15. Frangogiannis NG. Cell biological mechanisms in regulation of the post-infarction inflammatory response. Current Opinion in Physiology 2018; 1. doi:10.1016/j.cophys.2017.09.001.

16. Santos-Zas I, Lemarié J, Tedgui A, Ait-Oufella H. Adaptive Immune Responses Contribute to Post-ischemic Cardiac Remodeling. Front. Cardiovasc. Med. 2018; 5:198. doi:10.3389/fcvm.2018.00198.

17. Kologrivova I, Shtatolkina M, Suslova T, Ryabov V. Cells of the Immune System in Cardiac Remodeling: Main Players in Resolution of Inflammation and Repair After Myocardial Infarction. Frontiers in Immunology 2021; 12:664457. doi:10.3389/fimmu.2021.664457.

18. Heinrichs M, Ashour D, Siegel J, Büchner L, Wedekind G, Heinze KG et al. The healing myocardium mobilizes a distinct B-cell subset through a CXCL13-CXCR5-dependent mechanism. Cardiovasc Res 2021; 117(13):2664–76. doi:10.1093/cvr/cvab181.

19. van Taunay JS, Albelda MT, Frias JC, Lipinski MJ. Biologics and Cardiovascular Disease. Journal of Cardiovascular Pharmacology 2018; 72(2):77–85. doi:10.1097/FJC.0000000000000595.

20. Zouggari Y, Ait-Oufella H, Bonnin P, Simon T, Sage AP, Guérin C et al. B lymphocytes trigger monocyte mobilization and impair heart function after acute myocardial infarction. Nature Medicine 2013; 19(10):1273–80. doi:10.1038/nm.3284.

21. Prabhu SD, Frangogiannis NG. The biological basis for cardiac repair after myocardial infarction. 15244571; 2016. (vol 119).

22. Epelman S, Liu PP, Mann DL. Role of innate and adaptive immune mechanisms in cardiac injury and repair. 14741741; 2015. (vol 15).

23. Talman V, Ruskoaho H. Cardiac fibrosis in myocardial infarction—from repair and remodeling to regeneration. 14320878; 2016. (vol 365).

24. Ong SB, Hernández-Reséndiz S, Crespo-Avilan GE, Mukhametshina RT, Kwek XY, Cabrera-Fuentes HA et al. Inflammation following acute myocardial infarction: Multiple players, dynamic roles, and novel therapeutic opportunities. 1879016X; 2018. (vol 186).

25. Couto G de. Macrophages in cardiac repair: Environmental cues and therapeutic strategies. Exp Mol Med 2019; 51(12):1–10. doi:10.1038/s12276-019-0269-4.

26. Das A, Sinha M, Datta S, Abas M, Chaffee S, Sen CK et al. Monocyte and macrophage plasticity in tissue repair and regeneration. The American Journal of Pathology 2015; 185(10):2596–606. doi:10.1016/j.ajpath.2015.06.001.

27. Rech L, Rainer PP. The Innate Immune cGAS-STING-Pathway in Cardiovascular Diseases – A Mini Review. Front. Cardiovasc. Med. 2021; 8. doi:10.3389/fcvm.2021.715903.

28. Nidorf SM, Fiolet ATL, Mosterd A, Eikelboom JW, Schut A, Opstal TSJ et al. Colchicine in Patients with Chronic Coronary Disease. N Engl J Med 2020; 383(19):1838–47. doi:10.1056/NEJMoa2021372.

29. Tardif J-C, Kouz S, Waters DD, Bertrand OF, Diaz R, Maggioni AP et al. Efficacy and Safety of Low-Dose Colchicine after Myocardial Infarction. N Engl J Med 2019; 381(26):2497–505. doi:10.1056/NEJMoa1912388.

30. Mann DL. Innate immunity and the failing heart: the cytokine hypothesis revisited. Circulation Research 2015; 116(7):1254–68. doi:10.1161/CIRCRESAHA.116.302317.

31. Berry MF, Woo YJ, Pirolli TJ, Bish LT, Moise MA, Burdick JW et al. Administration of a tumor necrosis factor inhibitor at the time of myocardial infarction attenuates subsequent ventricular remodeling. J Heart Lung Transplant 2004; 23(9):1061–8. doi:10.1016/j.healun.2004.06.021.

32. Padfield GJ, Din JN, Koushiappi E, Mills NL, Robinson SD, Le Cruden NM et al. Cardiovascular effects of tumour necrosis factor α antagonism in patients with acute myocardial infarction: a first in human study. Heart 2013; 99(18):1330–5. doi:10.1136/heartjnl-2013-303648.

33. Adamo L, Rocha-Resende C, Prabhu SD, Mann DL. Reappraising the role of inflammation in heart failure. Nat Rev Cardiol 2020; 17(5):269–85. doi:10.1038/s41569-019-0315-x.

34. Fang L, Ellims AH, Beale AL, Taylor AJ, Murphy A, Dart AM. Systemic inflammation is associated with myocardial fibrosis, diastolic dysfunction, and cardiac hypertrophy in patients with hypertrophic cardiomyopathy 2017; 9(11):5063–73.

35. Aday AW, Ridker PM. Antiinflammatory Therapy in Clinical Care: The CANTOS Trial and Beyond. Front. Cardiovasc. Med. 2018; 5:62. doi:10.3389/fcvm.2018.00062.

36. Maimaitiaili A, Li J, Aibibula A, Abudureheman M. Inhibition of nuclear factor kappa B pathway protects myocardial ischemia/reperfusion injury in rats under treatment with abnormal savda munziq. Am J Transl Res 2018; 10(1):77–85.

37. Zhang XQ, Tang R, Li L, Szucsik A, Javan H, Saegusa N et al. Cardiomyocyte-specific p65 NF-κB deletion protects the injured heart by preservation of calcium handling. Am J Physiol Heart Circ Physiol 2013; 305(7):H1089-97. doi:10.1152/ajpheart.00067.2013.

38. Silvis MJM, Kaffka Genaamd Dengler SE, Odille CA, Mishra M, van der Kaaij NP, Doevendans PA et al. Damage-Associated Molecular Patterns in Myocardial Infarction and Heart Transplantation: The Road to Translational Success. Frontiers in Immunology 2020; 11:599511. doi:10.3389/fimmu.2020.599511.

39. Xu M, Liu PP, Li H. Innate Immune Signaling and Its Role in Metabolic and Cardiovascular Diseases. Physiol Rev 2019; 99(1):893–948. doi:10.1152/physrev.00065.2017.

40. Banete A, Seaver K, Bakshi D, Gee K, Basta S. On taking the STING out of immune activation. JOURNAL OF LEUKOCYTE BIOLOGY 2018. doi:10.1002/JLB.2MIR0917-383R.

41. Beutler B. Innate immunity: an overview. Molecular Immunology 2004; 40(12):845–59. doi:10.1016/j.molimm.2003.10.005.

42. Riera Romo M, Pérez-Martínez D, Castillo Ferrer C. Innate immunity in vertebrates: an overview. Immunology 2016; 148(2):125–39. doi:10.1111/imm.12597.

43. Tomar N, De RK. A brief outline of the immune system. Methods in molecular biology (Clifton, N.J.) 2014; 1184:3–12. doi:10.1007/978-1-4939-1115-8_1.

44. Medzhitov R. Origin and physiological roles of inflammation. Nature 2008; 454(7203):428–35. doi:10.1038/nature07201.

45. Akira S, Uematsu S, Takeuchi O. Pathogen recognition and innate immunity. Cell 2006; 124(4):783–801. doi:10.1016/j.cell.2006.02.015.

46. Schaefer L. Complexity of danger: the diverse nature of damage-associated molecular patterns. J. Biol. Chem. 2014; 289(51):35237–45. doi:10.1074/jbc.R114.619304.

47. Brzostek-Racine S, Gordon C, van Scoy S, Reich NC. The DNA damage response induces IFN. The Journal of Immunology 2011; 187(10):5336–45. doi:10.4049/jimmunol.1100040.

48. Zhong L, Hu M-M, Bian L-J, Liu Y, Chen Q, Shu H-B. Phosphorylation of cGAS by CDK1 impairs self-DNA sensing in mitosis. Cell Discov 2020; 6(1):26. doi:10.1038/s41421-020-0162-2.

49. Sun L, Wu J, Du F, Chen X, Chen ZJ. Cyclic GMP-AMP Synthase Is a Cytosolic DNA Sensor That Activates the Type I Interferon Pathway. Science 2013; 339(6121):786–91. doi:10.1126/science.1232458.

50. Schoggins JW, MacDuff DA, Imanaka N, Gainey MD, Shrestha B, Eitson JL et al. Pan-viral specificity of IFN-induced genes reveals new roles for cGAS in innate immunity. Nature 2014; 505(7485):691–5. doi:10.1038/nature12862.

51. Li X-D, Wu J, Gao D, Wang H, Sun L, Chen ZJ. Pivotal Roles of cGAS-cGAMP Signaling in Antiviral Defense and Immune Adjuvant Effects. Science 2013; 341(6152):1390–4. doi:10.1126/science.1244040.

52. Collins AC, Cai H, Li T, Franco LH, Li X-D, Nair VR et al. Cyclic GMP-AMP Synthase Is an Innate Immune DNA Sensor for Mycobacterium tuberculosis. Cell host & microbe 2015:820–8. doi:10.1016/j.chom.2015.05.005.

53. Civril F, Deimling T, Oliveira Mann CC de, Ablasser A, Moldt M, Witte G et al. Structural mechanism of cytosolic DNA sensing by cGAS. Nature 2013; 498(7454):332–7. doi:10.1038/nature12305.

54. Wu J, Sun L, Chen X, Du F, Shi H, Chen C et al. Cyclic GMP-AMP is an endogenous second messenger in innate immune signaling by cytosolic DNA. Science 2013; 339(6121):826–30. doi:10.1126/science.1229963.

55. Wan D, Jiang W, Hao J. Research Advances in How the cGAS-STING Pathway Controls the Cellular Inflammatory Response. Frontiers in Immunology 2020; 11:615. doi:10.3389/fimmu.2020.00615.

56. Liu H, Moura-Alves P, Pei G, Mollenkopf H-J, Hurwitz R, Wu X et al. cGAS facilitates sensing of extracellular cyclic dinucleotides to activate innate immunity. EMBO Rep 2019; 20(4). doi:10.15252/embr.201846293.

57. Yang H, Wang H, Ren J, Chen Q, Chen ZJ. cGAS is essential for cellular senescence. PNAS 2017; 114(23):E4612-E4620. doi:10.1073/pnas.1705499114.

58. Cai X, Chiu YH, Chen ZJ. The cGAS-cGAMP-STING pathway of cytosolic DNA sensing and signaling. 10974164; 2014. (vol 54).

59. Paludan SR, Bowie AG. Immune sensing of DNA. IMMUNITY 2013; 38(5):870–80. doi:10.1016/j.immuni.2013.05.004.

60. Chen Q, Sun L, Chen ZJ. Regulation and function of the cGAS–STING pathway of cytosolic DNA sensing. Nature Immunology 2016; 17(10):1142–9. doi:10.1038/ni.3558.

61. Barber GN. STING: infection, inflammation and cancer. Nat Rev Immunol 2015; 15(12):760–70. doi:10.1038/nri3921.

62. Ishikawa H, Barber GN. STING is an endoplasmic reticulum adaptor that facilitates innate immune signalling. Nature 2008; 455(7213):674–8. doi:10.1038/nature07317.

63. Haag SM, Gulen MF, Reymond L, Gibelin A, Abrami L, Decout A et al. Targeting STING with covalent small-molecule inhibitors. Nature 2018. doi:10.1038/s41586-018-0287-8.

64. Liu S, Cai X, Wu J, Cong Q, Chen X, Li T et al. Phosphorylation of innate immune adaptor proteins MAVS, STING, and TRIF induces IRF3 activation. Science 2015; 347(6227):aaa2630. doi:10.1126/science.aaa2630.

65. Tanaka Y, Chen ZJ. STING specifies IRF3 phosphorylation by TBK1 in the cytosolic DNA signaling pathway. Sci Signal 2012; 5(214):ra20. doi:10.1126/scisignal.2002521.

66. Burdette DL, Monroe KM, Sotelo-Troha K, Iwig JS, Eckert B, Hyodo M et al. STING is a direct innate immune sensor of cyclic di-GMP. Nature 2011; 478(7370):515–8. doi:10.1038/nature10429.

67. Liu Y-P, Zeng L, Tian A, Bomkamp A, Rivera D, Gutman D et al. Endoplasmic reticulum stress regulates the innate immunity critical transcription factor IRF3. The Journal of Immunology 2012; 189(9):4630–9. doi:10.4049/jimmunol.1102737.

68. Larkin B, Ilyukha V, Sorokin M, Buzdin A, Vannier E, Poltorak A. Cutting Edge: Activation of STING in T Cells Induces Type I IFN Responses and Cell Death. Journal of immunology (Baltimore, Md. : 1950) 2017; 199(2):397–402. doi:10.4049/jimmunol.1601999.

69. Gulen MF, Koch U, Haag SM, Schuler F, Apetoh L, Villunger A et al. Signalling strength determines proapoptotic functions of STING. Nature Communications 2017; 8(1). doi:10.1038/s41467-017-00573-w.

70. Tang C-HA, Zundell JA, Ranatunga S, Lin C, Nefedova Y, Del Valle JR et al. Agonist-Mediated Activation of STING Induces Apoptosis in Malignant B Cells: Single Nucleotide Polymorphisms of Human STING Can Affect Innate Immune Response to Cyclic Dinucleotides. CANCER RESEARCH 2016; 76(8):2137–52. doi:10.1158/0008-5472.CAN-15-1885.

71. Corrales L, Gajewski TF. Molecular Pathways: Targeting the Stimulator of Interferon Genes (STING) in the Immunotherapy of Cancer. Clinical cancer research : an official journal of the American Association for Cancer Research 2015; 21(21):4774–9. doi:10.1158/1078-0432.CCR-15-1362.

72. Weiss JM, Guérin MV, Regnier F, Renault G, Galy-Fauroux I, Vimeux L et al. The STING agonist DMXAA triggers a cooperation between T lymphocytes and myeloid cells that leads to tumor regression. Oncoimmunology 2017; 6(10):e1346765. doi:10.1080/2162402X.2017.1346765.

73. Guo F, Han Y, Zhao X, Wang J, Liu F, Xu C et al. STING Agonists Induce an Innate Antiviral Immune Response against Hepatitis B Virus; 2015. (vol 59).

74. Frémond M-L, Hadchouel A, Berteloot L, Melki I, Bresson V, Barnabei L et al. Overview of STING-Associated Vasculopathy with Onset in Infancy (SAVI) Among 21 Patients. J Allergy Clin Immunol Pract 2021; 9(2):803-818.e11. doi:10.1016/j.jaip.2020.11.007.

75. Ablasser A, Chen ZJ. cGAS in action: Expanding roles in immunity and inflammation. Science 2019; 363(6431). doi:10.1126/science.aat8657.

76. Li T, Chen ZJ. The cGAS-cGAMP-STING pathway connects DNA damage to inflammation, senescence, and cancer. The Journal of Experimental Medicine 2018; 215(5):1287–99. doi:10.1084/jem.20180139.

77. Ahn J, Gutman D, Saijo S, Barber GN. STING manifests self DNA-dependent inflammatory disease. Proceedings of the National Academy of Sciences 2012; 109(47):19386–91. doi:10.1073/pnas.1215006109.

78. Gao D, Li T, Li X-D, Chen X, Li Q-Z, Wight-Carter M et al. Activation of cyclic GMP-AMP synthase by self-DNA causes autoimmune diseases. Proc Natl Acad Sci U S A 2015; 112(42):E5699-705. doi:10.1073/pnas.1516465112.

79. Härtlova A, Erttmann SF, Raffi FA, Schmalz AM, Resch U, Anugula S et al. DNA Damage Primes the Type I Interferon System via the Cytosolic DNA Sensor STING to Promote Anti-Microbial Innate Immunity. IMMUNITY 2015; 42(2):332–43. doi:10.1016/j.immuni.2015.01.012.

80. Oduro PK, Zheng X, Wei J, Yang Y, Wang Y, Zhang H et al. The cGAS-STING signaling in cardiovascular and metabolic diseases: Future novel target option for pharmacotherapy. Acta Pharm Sin B 2022; 12(1):50–75. doi:10.1016/j.apsb.2021.05.011.

81. Decout A, Katz JD, Venkatraman S, Ablasser A. The cGAS-STING pathway as a therapeutic target in inflammatory diseases. 14741741 2021. doi:10.1038/s41577-021-00524-z.

82. Hall J, Brault A, Vincent F, Weng S, Wang H, Dumlao D et al. Discovery of PF-06928215 as a high affinity inhibitor of cGAS enabled by a novel fluorescence polarization assay. PLoS ONE 2017; 12(9):e0184843. doi:10.1371/journal.pone.0184843.

83. Vincent J, Adura C, Gao P, Luz A, Lama L, Asano Y et al. Small molecule inhibition of cGAS reduces interferon expression in primary macrophages from autoimmune mice. Nature Communications 2017; 8(1):750. doi:10.1038/s41467-017-00833-9.

84. Rech L, Abdellatif M, Pöttler M, Stangl V, Mabotuwana N, Hardy S et al. Small molecule STING inhibition improves myocardial infarction remodeling. Life Sci 2021; 291:120263. doi:10.1016/j.lfs.2021.120263.

85. Li N, Zhou H, Wu H, Wu Q, Duan M, Deng W et al. STING-IRF3 contributes to lipopolysaccharide-induced cardiac dysfunction, inflammation, apoptosis and pyroptosis by activating NLRP3. Redox Biol 2019; 24:101215. doi:10.1016/j.redox.2019.101215.

86. Xu Q., Xiong H., Zhu W., Liu Y., Du Y. Small molecule inhibition of cyclic GMP-AMP synthase ameliorates sepsis-induced cardiac dysfunction in mice. Life Sciences. 260 (no pagination), 2020. Article Number: 118315. Date of Publication: 1 November 2020. 2020. doi:10.1016/j.lfs.2020.118315.

87. Choudhuri S, Garg NJ. PARP1-cGAS-NF-kappa B pathway of proinflammatory macrophage activation by extracellular vesicles released during Trypanosoma cruzi infection and Chagas disease. PLOS PATHOGENS 2020; 16(4). doi:10.1371/journal.ppat.1008474.

88. Berthelot J-M, Lioté F, Maugars Y, Sibilia J. Lymphocyte Changes in Severe COVID-19: Delayed Over-Activation of STING? Frontiers in Immunology 2020; 11:607069. doi:10.3389/fimmu.2020.607069.

89. Basso C, Leone O, Rizzo S, Gaspari M de, van der Wal AC, Aubry M-C et al. Pathological features of COVID-19-associated myocardial injury: a multicentre cardiovascular pathology study. European Heart Journal 2020; 41(39):3827–35. doi:10.1093/eurheartj/ehaa664.

90. Di Domizio J, Gulen MF, Saidoune F, Thacker VV, Yatim A, Sharma K et al. The cGAS-STING pathway drives type I IFN immunopathology in COVID-19. Nature 2022; 603(7899):145–51. doi:10.1038/s41586-022-04421-w.

91. Liu X, Wei L, Xu F, Zhao F, Huang Y, Fan Z et al. SARS-CoV-2 spike protein–induced cell fusion activates the cGAS-STING pathway and the interferon response. Sci Signal 2022; 15(729). doi:10.1126/scisignal.abg8744.

92. Ponikowski P, Voors AA, Anker SD, Bueno H, Cleland JGF, Coats AJS et al. 2016 ESC Guidelines for the diagnosis and treatment of acute and chronic heart failure: The Task Force for the diagnosis and treatment of acute and chronic heart failure of the European Society of Cardiology (ESC)Developed with the special contribution of the

Heart Failure Association (HFA) of the ESC. Eur Heart J 2016; 37(27):2129–200. doi:10.1093/eurheartj/ehw128.

93. deAlmeida AC, van Oort RJ, Wehrens XHT. Transverse aortic constriction in mice. Journal of visualized experiments : JoVE 2010; (38). doi:10.3791/1729.

94. Liu Y, Leri A, Li B, Wang X, Cheng W, Kajstura J et al. Angiotensin II stimulation in vitro induces hypertrophy of normal and postinfarcted ventricular myocytes. Circulation Research 1998; 82(11):1145–59. doi:10.1161/01.RES.82.11.1145.

95. Zhang Y, Chen W, Wang Y. STING is an essential regulator of heart inflammation and fibrosis in mice with pathological cardiac hypertrophy via endoplasmic reticulum (ER) stress. Biomed Pharmacother 2020; 125:110022. doi:10.1016/j.biopha.2020.110022.

96. Hu D, Cui Y-X, Wu M-Y, Li L, Su L-N, Lian Z et al. Cytosolic DNA sensor cGAS plays an essential pathogenetic role in pressure overload-induced heart failure. American Journal of Physiology - Heart and Circulatory Physiology 2020; 318(6):H1525-H1537. doi:10.1152/ajpheart.00097.2020.

97. Yan M, Li Y, Luo Q, Zeng W, Shao X, Li L et al. Mitochondrial damage and activation of the cytosolic DNA sensor cGAS-STING pathway lead to cardiac pyroptosis and hypertrophy in diabetic cardiomyopathy mice. Cell Death Discov 2022; 8(1):258. doi:10.1038/s41420-022-01046-w.

98. Cao DJ, Schiattarella GG, Villalobos E, Jiang N, May HI, Li T et al. Cytosolic DNA Sensing Promotes Macrophage Transformation and Governs Myocardial Ischemic Injury. Circulation 2018; 137(24):2613–34. doi:10.1161/CIRCULATIONAHA.117.031046.

99. King KR, Aguirre AD, Ye YX, Sun Y, Roh JD, Ng RP et al. IRF3 and type I interferons fuel a fatal response to myocardial infarction. Nature Medicine 2017; 23(12):1481–7. doi:10.1038/nm.4428.

100. Hu S, Gao Y, Gao R, Wang Y, Qu Y, Yang J et al. The selective STING inhibitor H-151 preserves myocardial function and ameliorates cardiac fibrosis in murine myocardial infarction. International Immunopharmacology 2022; 107:108658. doi:10.1016/j.intimp.2022.108658.

101. Orecchioni M, Ghosheh Y, Pramod AB, Ley K. Macrophage Polarization: Different Gene Signatures in M1(LPS+) vs. Classically and M2(LPS-) vs. Alternatively Activated Macrophages. Frontiers in Immunology 2019; 10:1084. doi:10.3389/fimmu.2019.01084.

102. Ablasser A, Goldeck M, Cavlar T, Deimling T, Witte G, Röhl I et al. CGAS produces a 2′-5′-linked cyclic dinucleotide second messenger that activates STING. Nature 2013; 498(7454):380–4. doi:10.1038/nature12306.

103. Li Q, Cao Y, Dang C, Han B, Han R, Ma H et al. Inhibition of double-strand DNA-sensing cGAS ameliorates brain injury after ischemic stroke. EMBO Mol Med 2020; 12(4):e11002. doi:10.15252/emmm.201911002.

104. Guillen J. FELASA guidelines and recommendations. J Am Assoc Lab Anim Sci; 2012. (vol 51).

105. Voipio H-M, Baneux P, Gomez de Segura IA, Hau J, Wolfensohn S. Guidelines for the veterinary care of laboratory animals: report of the FELASA/ECLAM/ESLAV Joint Working Group on Veterinary Care. Lab Anim 2008; 42(1):1–11. doi:10.1258/la.2007.007027.

106. ARRIVE Guidelines. Available from: URL: https://arriveguidelines.org/.

107. Wang L, Xie L, Zhang Q, Cai X, Tang Y, Wang L et al. Plasma nuclear and mitochondrial DNA levels in acute myocardial infarction patients. Coron Artery Dis 2015; 26(4):296–300. doi:10.1097/MCA.0000000000000231.

108. ter Horst EN, Krijnen PAJ, Hakimzadeh N, Robbers LFHJ, Hirsch A, Nijveldt R et al. Elevated monocyte-specific type I interferon signalling correlates positively with cardiac healing in myocardial infarct patients but interferon alpha application deteriorates myocardial healing in rats. Basic Research in Cardiology 2018; 114(1):1. doi:10.1007/s00395-018-0709-7.

109. Benavides-Vallve C, Corbacho D, Iglesias-Garcia O, Pelacho B, Albiasu E, Castaño S et al. New strategies for echocardiographic evaluation of left ventricular function in a mouse model of long-term myocardial infarction. PLoS ONE 2012; 7(7):e41691. doi:10.1371/journal.pone.0041691.

110. Hinton RB, Alfieri CM, Witt SA, Glascock BJ, Khoury PR, Benson DW et al. Mouse heart valve structure and function: echocardiographic and morphometric analyses from the fetus through the aged adult. AMERICAN JOURNAL OF PHYSIOLOGY-HEART AND CIRCULATORY PHYSIOLOGY 2008; 294(6):H2480-8. doi:10.1152/ajpheart.91431.2007.

111. Yang XP, Liu YH, Rhaleb NE, Kurihara N, Kim HE, Carretero OA. Echocardiographic assessment of cardiac function in conscious and anesthetized mice. Am J Physiol 1999; 277(5):H1967-74. doi:10.1152/ajpheart.1999.277.5.H1967.

112. Lindsey ML, Kassiri Z, Virag JAI, Castro Bras LE de, Scherrer-Crosbie M. Guidelines for Measuring Cardiac Physiology in Mice. AMERICAN JOURNAL OF PHYSIOLOGY-HEART AND CIRCULATORY PHYSIOLOGY 2018; 314(4). doi:10.1152/ajpheart.00339.2017.

113. Gao E, Lei YH, Shang X, Huang ZM, Zuo L, Boucher M et al. A novel and efficient model of coronary artery ligation and myocardial infarction in the mouse. 15244571 2010; 107(12):1445–53. doi:10.1161/CIRCRESAHA.110.223925.

114. Hoog VC de, Bovens SM, Jager SCA de, van Middelaar BJ, van Duijvenvoorde A, Doevendans PA et al. BLT1 antagonist LSN2792613 reduces infarct size in a mouse model of myocardial ischaemia-reperfusion injury. Cardiovasc Res 2015; 108(3):367–76. doi:10.1093/cvr/cvv224.

115. Villiers C de, Riley PR. Mouse models of myocardial infarction: comparing permanent ligation and ischaemia-reperfusion. Disease Models & Mechanisms 2020; 13(11). doi:10.1242/dmm.046565.

116. Montorfano I, Becerra A, Cerro R, Echeverría C, Sáez E, Morales MG et al. Oxidative stress mediates the conversion of endothelial cells into myofibroblasts via a

TGF-β1 and TGF-β2-dependent pathway. Lab Invest 2014; 94(10):1068–82. doi:10.1038/labinvest.2014.100.

117. Ma J, Sanchez-Duffhues G, Goumans M-J, Dijke P ten. TGF-β-Induced Endothelial to Mesenchymal Transition in Disease and Tissue Engineering. Front Cell Dev Biol 2020; 8:260. doi:10.3389/fcell.2020.00260.

118. Alonso-Herranz L, Sahún-Español Á, Paredes A, Gonzalo P, Gkontra P, Núñez V et al. Macrophages promote endothelial-to-mesenchymal transition via MT1-MMP/TGFβ1 after myocardial infarction. eLife 2020; 9. doi:10.7554/eLife.57920.

119. Hanna A, Frangogiannis NG. The Role of the TGF-β Superfamily in Myocardial Infarction. Front. Cardiovasc. Med. 2019; 6:140. doi:10.3389/fcvm.2019.00140.

120. Zhang F, Wang H, Wang X, Jiang G, Liu H, Zhang G et al. TGF-β induces M2-like macrophage polarization via SNAIL-mediated suppression of a pro-inflammatory phenotype. Oncotarget 2016; 7(32):52294–306. doi:10.18632/oncotarget.10561.

121. Huang J, Pu Y, Zhang H, Xie L, He L, Zhang C-L et al. KLF2 Mediates the Suppressive Effect of Laminar Flow on Vascular Calcification by Inhibiting Endothelial BMP/SMAD1/5 Signaling. 15244571 2021; 129(4):e87-e100. doi:10.1161/CIRCRESAHA.120.318690.

122. Essani NA, Fisher MA, Jaeschke H. Inhibition of NF-kappa B activation by dimethyl sulfoxide correlates with suppression of TNF-alpha formation, reduced ICAM-1 gene transcription, and protection against endotoxin-induced liver injury. Shock 1997; 7(2):90–6. doi:10.1097/00024382-199702000-00003.

123. Grunwell JR, Yeligar SM, Stephenson S, Du Ping X, Gauthier TW, Fitzpatrick AM et al. TGF-β1 Suppresses the Type I IFN Response and Induces Mitochondrial Dysfunction in Alveolar Macrophages. J.I. 2018; 200(6):2115–28. doi:10.4049/jimmunol.1701325.

124. Bujak M, Frangogiannis NG. The role of TGF-beta signaling in myocardial infarction and cardiac remodeling. CARDIOVASCULAR RESEARCH 2007; 74(2):184–95. doi:10.1016/j.cardiores.2006.10.002.

125. Desmoulière A, Geinoz A, Gabbiani F, Gabbiani G. Transforming growth factor-beta 1 induces alpha-smooth muscle actin expression in granulation tissue myofibroblasts and in quiescent and growing cultured fibroblasts. J Cell Biol 1993; 122(1):103–11. doi:10.1083/jcb.122.1.103.

126. Elisia I, Nakamura H, Lam V, Hofs E, Cederberg R, Cait J et al. DMSO Represses Inflammatory Cytokine Production from Human Blood Cells and Reduces Autoimmune Arthritis. PLoS ONE 2016; 11(3):e0152538. doi:10.1371/journal.pone.0152538.

127. Kramer K, van Acker SA, Grimbergen JA, van den Berg D-J, van der Vijgh WJ, Bast A. Effect of dimethyl sulfoxide (DMSO) on the electrocardiogram (ECG) in freely moving male Balb/c mice. General Pharmacology: The Vascular System 1995; 26(6):1403–7. doi:10.1016/0306-3623(94)00300-c.

7 Protocols and supplemental data

7.1 Histology – HE staining

Slice from FFPE

1. Deparaffinize and rehydration
    a. 2x2 min Xylol
    b. 2 min 100% Ethanol
    c. 2 min 90% Ethanol
    d. 2 min 70% Ethanol
    e. 2 min 50% Ethanol
    f. 2 min dH_2O
2. Staining
    a. 4 min Haematoxylin
    b. 2 min hot water rinsing
    c. 4 min Eosin
3. Dehydration
    a. 2x2 min dH_2O
    b. 2 min 50% Ethanol
    c. 2 min 70% Ethanol
    d. 2 min 90% Ethanol
    e. 2 min 100% Ethanol
    f. 2x2 min Xylol
4. Coverslip

7.2 Fluorescence staining – WGA

Slices from FFPE

1. Deparaffinize and rehydration
    a. 2x5 min Xylol
    b. 5 min 100% Ethanol
    c. 5 min 90% Ethanol
    d. 5 min 70% Ethanol
    e. 5 min 50% Ethanol
    f. 5 min dH_2O
2. Antigen Retrieval
    a. Boil in sodium-citrate buffer (Na-Citrate, 0.05% Tween20, pH6) for 15 min in microwave full power, slices covered
    b. Cool slices over 5 min by running dH_2O into the chamber
    c. Put in dH_2O jar
3. Marking slices with SuperPap Pen and put in PBS
4. Staining
    a. Dilute WGA stock in PBS (1:200)
    b. Put 100 µl on each marked spot and incubate 1h at room temperature
    c. Washing: rise 3x5 min with PBS
5. Coverslip with mounting media, dry in the dark (12-24h) and seal coverslip with nail polish

7.3 RNA isolation and purification with RNeasy kit (QIAGEN) and DNase digestion (QIAGEN)

1. Tissue samples from storage use. Not more than 50 mg
2. Measure the weight of tissue. Add 700 µl QIAzol lysis reagent in a tube (part of the kit)
3. Homogenise in a MagnaLyser, with tubes from MagnaLyser beats.
   4 x 17sec with 6500rpm, between 2 min break on ice
4. Place at room temperature for 5 min
5. Add 140 µl chloroform and shake for 15sec
6. Place at room temperature for 2-3 min
7. Centrifuge 15 min with 12.000g at 4°C
8. Transfer the upper aqueous phase to a new tube (measure volume).
   Add 1.5x volume of 100% ethanol and mix by pipetting up and down.
   Continue without delay
   Pipet up to 700 µl of sample solution into an RNeasy Mini Spin column in a collection tube.
   Centrifuge at 10.000 rpm for 15 sec. at room temperature
9. Repeat step 9 with the rest of the sample
10. Pipet 700 µl RWT Buffer into spin column and centrifuge for 15 sec. at 10.000 rpm
11. Add 10 µl DNase 1 Stock solution to 70 µl RDD Buffer (for each sample) and mix gently (not vortex)
12. Pipet DNase 1 mix 80 µl directly onto the spin column membrane and place at 20-30°C for 15 min.
13. Pipet 350 µl RWT Buffer on spin column and centrifuge for 15 sec. at 10.000 rpm
14. Pipet 500 µl RPE Buffer into the spin column and centrifugate at 10.000 rpm for 15 sec.
15. Pipet 500 µl RPE Buffer into the spin column and centrifugate at 10.000 rpm for 2 min to dry the spine column membrane.
16. Place spine column into a new collection tube and centrifugate at full speed for 1 min.
17. Transfer spine column on a final tube.
    Add 30myl RNAse-free water directly onto the spine column membrane.
    Centrifuge for 1 min at 10.000 rpm.
18. If expected, RNA yield >30 µg repeat step 18.

7.4 cDNA synthesis for 20 µl volume with QIAgen RT-KIT

1. Take x µl RNA for 1 µg inside
2. Add dH_2O up to 12 µl
3. Add 2 µl Wipeout Buffer
4. Place in a thermocycler for 2 min at 42°C. Afterwards, place directly on ice
5. Add 6 µl RT-Mastermix
    a. RT-Mastermix
        i. Reverse transcriptase 1 µl
        ii. RT Buffer 4 µl
        iii. RT Primer Mix 1 µl
    b. RT-Minus Control
        i. dH_2O 1 µl
        ii. RT Buffer 4 µl
        iii. RT Primer Mix 1 µl
6. Centrifuge short to eliminate air bubbles
7. Place in thermocycler
    a. 42°C for 15-30 min (for 1 µg 30 min)
    b. 95°C for 3 min

7.5 Protocol qPCR

Total sample volume each well: 10 µl

dH_2O	0.48 µl
SYBR green Master Mix	5.00 µl
Forward primer (260 nM)	0.26 µl
Reverse primer (260 nM)	0.26 µl
cDNA	4.00 µl

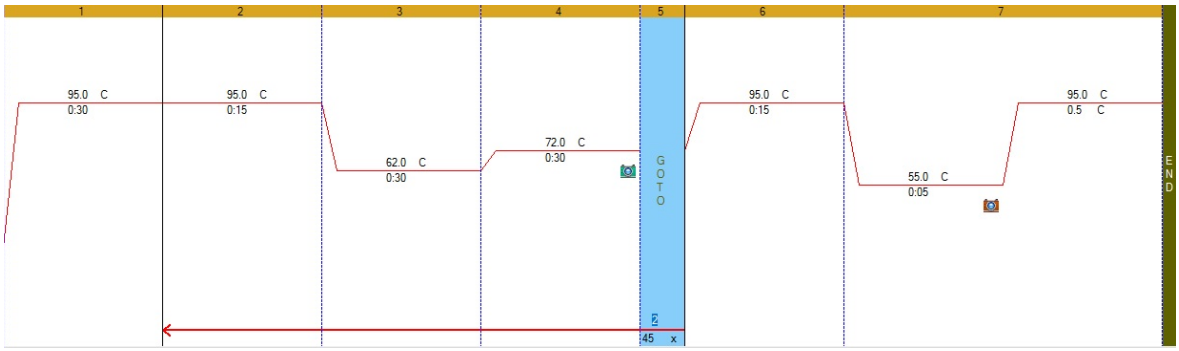

Figure 27: qPCR running protocol

7.6 Primer Efficiencies

Gene	Efficiency [%]
Il6	103.2
Nppa	96.6
Nppb	97.3
Myh6	95.2
Tnfα	105.4
Tgfβ1	99.0
Tgfβ2	95.8
Myh7	100.7
Ifit2	100.4
Ifi44	97.8
Il1β	108.8
Cxcl10	101.5
Isg15	95.3
Col1a1	110.8
Col3a1	103.0
Col1a2	108.7
Hmbs	101.3
18s	102.0

7.7 Comprehensible assessment of the degree of stress for mice

BioMed RESEARCH GRAZ

Ermittlung des Belastungsgrades im Tierversuch: Abteilung Biomedizinische Forschung

Beobachtung	**Punktebewertung**
I Körpergewicht	
-unbeeinflusst	0
-Änderung < 5%	1
-Gewichtsreduktion 5-10%	5
-Gewichtsreduktion 11-20%	10
-Gewichtsreduktion >20%	20
II Allgemeinzustand	
-Fell glatt, glänzend; Körperöffnung sauber; Augen klar, glänzend	0
-Felldefekte (verminderte oder übersteigerte Körperpflege)	1
-Fell stumpf, ungeordnet, ungepflegte Körperöffnungen, Veränderung der Hautoberfläche (kleine Wunden), Augen trüb bzw. Augenausfluss, geringgradiger Rektalprolaps, unnormale Haltung, erhöhter Muskeltonus	5
-Schmutziges Fell, verklebte Körperöffnungen, mittelgradiger Rektalprolaps, dehydriert, abnormale Haltung, erhöhter Muskeltonus	10
-Verkrampfung, Lähmung (Rumpfmuskulatur, Extremitäten); Atemgeräusche; Rektalprolaps hochgradig ausgebildet	20
III Spontanverhalten	
-normales Verhalten (Schlafen, Reaktion auf Anblasen und Berührung, Neugier, Sozialkontakte)	0
-geringe Abweichung vom Normalverhalten	1
-ungewöhnliches Verhalten, eingeschränkte Motorik oder Hyperkinetik	5
-Selbstisolation, Lethargie; ausgeprägte Hyperkinetik bzw. Verhaltensstereotypien; Koordinationsstörungen	10
-Schmerzlaute beim Ergreifen; Selbstamputation (Autoaggression)	20
IV Klinischer Befund	
-Temperatur und Atmung normal, Extremitäten warm, Schleimhäute gut durchblutet, Abdomen physiologische Wirkung	0
-geringe Abweichung von Normalsituation	1
-Tier fühlt sich kälter an als normal, Extremitäten sind kalt, Schleimhäute sind blass	5
- Atemfrequenz + oder -30%, umfangsvermehrtes Abdomen	10
- Tier ist kalt, Schleimhäute blass, Atemfrequenz + oder -50%,	20

Blut im Urin oder Kot	
V Studien spezifische Abbruchkriterien	
- Geringgradiger Adaptationsdefekt der Wundränder, Nicht-eitrige Sekretion aus dem Bereich der Wunde	10
- Deutliches Klaffen der Wundränder, Eitrige Sekretion aus dem Wundbereich	20
- Geringgradige ausgeprägte Ödeme an den Extremitäten	10
- Stark ausgeprägte generalisierte Ödeme	20
Bewertung, Maßnahmen	
Belastungsgrad 0= keine Belastung	0
Belastungsgrad 1= geringe Belastung, sorgfältig weiter Beobachten	1-9
Belastungsgrad 2= mittelgradige Belastung, der Tierarzt muss informiert werden, ggf. tierärztliche Versorgung einleiten	10-19
Belastungsgrad 3= hochgradige Belastung, bei mehrtägiger Andauer der Belastung – der Tierarzt und der Studiendirektor müssen informiert werden- tierärztliche Versorgung einleiten, ggf. Tier einschläfern bzw. Versuch abbrechen	20 oder mehr

Kontakt: Mag. Beate Obermüller
Letzte Änderung: 12.10.2017

8 Equipment and expendable items

Table 6: Devices and Software

	Label	Company	Country
Devices	SZX microscope	Olympus	Japan
	MiniVent Type 845	Hugo Sachs Elektronik	Germany
	TC-1000 heating pad	CWE Inc.	United States
	Animal Bio Amp. FE136 (ECG)	ADInstruments	Austalia
	VisualSonic mouse table	VisualSonic Inc.	Canada
	Vevo 770 Imaging	VisualSonic Inc.	Canada
	RMV 707B transducer	VisualSonic Inc.	Canada
	Zivic matrix heart slicer	Zivic Instruments	United States
	SZX12 microscope	Olympus	Japan
	DP21 camera	Olympus	Japan
	Nanodrop 2000c	Thermo Fisher Scientific	United States
	CFX384 Detection system	Bio-Rad	Japan
	CFX96 Detection System	Bio-Rad	Japan
	Rotation microtome HM355S	Thermo Fisher Scientific	United States
	BX51 fluorescence microscope	Olympus	Japan
	CY3 filter (513-556 nm)	Olympus	Japan
	MagnaLyser	Roche	Swiss
Sofware	GraphPad Prism 8 software	GraphPad Software Inc.	United States
	ImageJ software	National Institue of Health	United States
	CaseViewer 2.4 software	3DHISTECH Ltd.	Hungary
	CFX Manager	Bio-Red	Japan
	GIMP 2.10	The DIMP Team	

Table 7: Reagents, Kits and Material

	Label	Description	Company	Country	ordering number/codes
Reagents	Isofluran	Isofluran-Piramal	Piramal Critical Care	United Kingdom	ATC-Code: N01AB06
	Etomidate	Hypnomidate	Janssen-Cilag Pharma GmbH	Austria	ATC-Code: N01AX07
	Buprenorphine	Bupaq	Richter Pharme AG	Austria	ATC-Code: QN02AE01
	Tween80		Sigma-Aldrich	United States	P4780
	Isotonic saline solution		Fresenius Kabi	Germany	PZN: 03236364
	Dimethylsulfoxid (DMSO)		Carl Roth	Germany	4720
	STING inhibitor	Inhibitor B, Inhibitor H-151		Lausanne	provided by Prof. A. Ablasser
	Heparine	Heparin Gilvasan	Gilvasan Pharma GmbH	Austria	ATC-Code: B01AB01
	Phosphate-buffered saline (PBS)		Sigma-Aldrich	United States	79382
	Evans blue		Sigma-Aldrich	United States	E2129
	2,3,5-Triphenyl-2H-tetrazolium chloride (TTC)		Alfa Aesar	United States	A10870
	QIAzol lysis reagent		QIAGEN	Netherland	79306
	SsoAdvanced Universal SYBR Green Supermix		Bio-Rad	Japan	1725271
	Sodium citrate		Sigma-Aldrich	United States	W302600
	Tween20		Sigma-Aldrich	United States	P1379
	Wheat germ agglutination (WGA) fluoresence conjugate	WGA, Alexa fluor 555	Invitrogen	United States	W32464
	GLC mounting medium		Sakua Finetek	Japan	1408
	Formalin aldehyde after Lillie 4%		Donauchem	Austria	4203601
	Ethanol	Ethanol absolute for analysis EMSURE® ACS,ISO,Reag. Ph Eur	Merck Millipore	USA	EC-Index-number: 603-002-00-5
	Chloroform	Chloroform for analysis EMSURE® ACS,ISO,Reag. Ph Eur	Merck Millipore	USA	EC-Index-number: 602-006-00-4
	Depilatory creme		Veet	Austria	
	Bepanthen eye and nose ointment	Dexpanthenol	Bayer Vital GmbH	Germany	ATC-Code: D03AX03
Kits	RNeasy kit		QIAGEN	Netherland	74104
	QuantiTect Reverse Transcription Kit		QIAGEN	Netherland	205311
Material	Prolene	7-0 monofilament Prolene	Ethicon Inc.	United States	KHH5673SH
	Prolene	6-0 monofilament Prolene	Ethicon Inc.	United States	EH8030H
	Magna Lyser Tubes	MagNA Lyser Green Beads	Roche Molecular Systems Inc.	United States	3358941001
	384 well Plate qPCR	Hard-Shell® 384-Well PCR Plates, thin wall, skirted, clear/white	Bio-Rad	Japan	HSP3805
	96 well Plate qPCR	Hard-Shell® 96-Well PCR Plates, low profile, thin wall, skirted, white/white	Bio-Rad	Japan	HSP9655